The High-Resolution Rapid Refresh (HRRR): An Hourly Updating Convection-Allowing Forecast Model. Part I: Motivation and System Description

DAVID C. DOWELL,[a] CURTIS R. ALEXANDER,[a] ERIC P. JAMES,[b,a] STEPHEN S. WEYGANDT,[a] STANLEY G. BENJAMIN,[a] GEOFFREY S. MANIKIN,[c] BENJAMIN T. BLAKE,[d,c] JOHN M. BROWN,[a] JOSEPH B. OLSON,[a] MING HU,[a] TATIANA G. SMIRNOVA,[b,a] TERRA LADWIG,[a] JAYMES S. KENYON,[b,a] RAVAN AHMADOV,[b,a] DAVID D. TURNER,[a] JEFFREY D. DUDA,[b,a] AND TREVOR I. ALCOTT[a]

[a] *NOAA/Global Systems Laboratory, Boulder, Colorado*
[b] *Cooperative Institute for Research in Environmental Sciences, University of Colorado Boulder, Boulder, Colorado*
[c] *NOAA/Environmental Modeling Center, College Park, Maryland*
[d] *I. M. Systems Group, Inc., Rockville, Maryland*

ABSTRACT: The High-Resolution Rapid Refresh (HRRR) is a convection-allowing implementation of the Advanced Research version of the Weather Research and Forecasting (WRF-ARW) Model with hourly data assimilation that covers the conterminous United States and Alaska and runs in real time at the NOAA/National Centers for Environmental Prediction (NCEP). Implemented operationally at NOAA/NCEP in 2014, the HRRR features 3-km horizontal grid spacing and frequent forecasts (hourly for CONUS and 3-hourly for Alaska). HRRR initialization is designed for optimal short-range forecast skill with a particular focus on the evolution of precipitating systems. Key components of the initialization are radar-reflectivity data assimilation, hybrid ensemble-variational assimilation of conventional weather observations, and a cloud analysis to initialize stratiform cloud layers. From this initial state, HRRR forecasts are produced out to 18 h every hour, and out to 48 h every 6 h, with boundary conditions provided by the Rapid Refresh system. Between 2014 and 2020, HRRR development was focused on reducing model bias errors and improving forecast realism and accuracy. Improved representation of the planetary boundary layer, subgrid-scale clouds, and land surface contributed extensively to overall HRRR improvements. The final version of the HRRR (HRRRv4), implemented in late 2020, also features hybrid data assimilation using flow-dependent covariances from a 3-km, 36-member ensemble ("HRRRDAS") with explicit convective storms. HRRRv4 also includes prediction of wildfire smoke plumes. The HRRR provides a baseline capability for evaluating NOAA's next-generation Rapid Refresh Forecast System, now under development.

SIGNIFICANCE STATEMENT: NOAA's operational hourly updating, convection-allowing model, the High-Resolution Rapid Refresh (HRRR), is a key tool for short-range weather forecasting and situational awareness. Improvements in assimilation of weather observations, as well as in physics parameterizations, have led to improvements in simulated radar reflectivity and quantitative precipitation forecasts since the initial implementation of HRRR in September 2014. Other targeted development has focused on improved representation of the diurnal cycle of the planetary boundary layer, resulting in improved near-surface temperature and humidity forecasts. Additional physics and data assimilation changes have led to improved treatment of the development and erosion of low-level clouds, including subgrid-scale clouds. The final version of HRRR features storm-scale ensemble data assimilation and explicit prediction of wildfire smoke plumes.

KEYWORDS: Cloud resolving models; Operational forecasting; Numerical weather prediction/forecasting; Regional models

---

1. Introduction

Over the past few decades, operational numerical weather prediction in the United States, and indeed around the world, has advanced significantly in terms of data assimilation (DA) and model complexity (e.g., Wang and Lei 2014; Gustafsson et al. 2018; Gross et al. 2018), as well as toward finer model horizontal grid spacing (e.g., Brown et al. 2012). The advent of convection-allowing models (CAMs; Table 1), having

sufficiently fine horizontal resolution to produce explicit deep, moist convection, allows more accurate forecasts of high-impact weather (e.g., Done et al. 2004; Weisman et al. 2008; Kain et al. 2008). In addition, rapidly updating NWP systems, able to take advantage of the latest weather observations, form a critical component of situational awareness and short-range (0–48 h) forecast guidance for quickly evolving weather events (e.g., Sun et al. 2014; Benjamin et al. 2016, hereafter B16; Simonin et al. 2017).

Given the need for accurate, short-range, fine-scale forecasts, NOAA has developed the High-Resolution Rapid Refresh (HRRR), an hourly updating, convection-allowing

---

ᶚ Denotes content that is immediately available upon publication as open access.

Corresponding author: David C. Dowell, David.Dowell@noaa.gov

TABLE 1. International operational regional non-hydrostatic NWP systems applied at a horizontal grid spacing of ≤5 km as of late 2020. (Adapted from Benjamin et al. 2019, their Table 13-8.)

NWP system	Center	Grid spacing/No. of layers	Initialization frequency	Frequency for free forecast	Current data assimilation method	Use of radar data	Operational since	Reference(s)
HRRR	NCEP, United States	3 km/L51	1 h	1 h	Hybrid 3D EnVar (HRRRv4)	Latent heating; EnKF	Sep 2014	This manuscript; James et al. (2022); Weygandt et al. (2022)
HRDPS	ECCC, Canada	2.5 km/L62	6 h	6 h	Downscaled from 10-km EnVar	None	Nov 2014	Milbrandt et al. (2016)
UKV	Met Office, United Kingdom	1.5 km/L70	1 h	1 h	4DVar	Latent heat nudging	2009	Tang et al. (2013)
AROME-France	Météo-France	1.3 km/L90	1 h	3 h	3DVar	Assimilation of pseudo-RH from radar	Dec 2008	Seity et al. (2011); Wattrelot et al. (2014); Brousseau et al. (2016)
COSMO-DE	DWD, Germany	2.2 km/L65	1 h	3 h	Nudging-LETKF	Latent heat nudging	Apr 2007	Baldauf et al. (2011); Schraff et al. (2016)
LFM	JMA, Japan	2 km/L58	1 h	1 h	3DVar	Assimilation of RH from radar and radial wind	Mar 2013	Saito et al. (2006)

model with 3-km horizontal grid spacing, based on a framework of community-supported data-assimilation and forecast-model infrastructure. The HRRR provides guidance for rapidly evolving mesoscale weather phenomena, including convective storms, mesoscale snow bands, tropical cyclones, downslope windstorms, fog and low cloud ceilings, intense cold fronts, dense smoke plumes from active wildfires, and rapid changes (ramps) in wind and solar energy sources. These local, rapidly evolving phenomena dramatically affect many sectors of society including the everyday lives of the public. The wide range of high-impact weather events forecast by the HRRR is represented in Fig. 1: composite radar reflectivity in tornadic supercell thunderstorms impacting the Dallas–Fort Worth metropolitan area (Fig. 1a); snow accumulation from a lake-effect snowstorm over the lower Great Lakes region (Fig. 1b); 80-m wind speeds up to and exceeding 90 kt (1 kt ≈ 0.51 m s^{-1}) associated with a severe Midwest derecho (Fig. 1c); and near-surface smoke near the Camp Fire in northern California (Fig. 1d).

An essential feature of the HRRR system is its rapid (hourly) updates useful for assimilating the latest weather observations (B16); the HRRR assimilates all conventional observations (aircraft, rawinsonde, GPS precipitable water, surface, buoy/ship, profiler, and satellite winds) used for the Rapid Refresh (RAP), as well as three-dimensional

radar-reflectivity observations provided through the NOAA Multi-Radar Multi-Sensor project (MRMS; Zhang et al. 2016; Smith et al. 2016; Kelleher et al. 2007). A radar-based latent-heating technique used for all HRRR versions (Weygandt et al. 2022), complemented by the more recent 3-km ensemble DA in HRRRv4, is described in this paper in section 3d. Availability of the frequently updated MRMS radar reflectivity mosaic over the entire country is a key enabler for the success of the HRRR. Assimilation of these radar observations is particularly critical for convective-storm forecasts in which the environment is often evolving and skill decreases rapidly with forecast lead time (Sun et al. 2014).

The NOAA Global Systems Laboratory (GSL) developed initial versions of an experimental HRRR as a real-time demonstration tool for short-range thunderstorm forecast guidance for severe weather and for aviation routing, using initial and boundary conditions from the Rapid Update Cycle (RUC) in 2008–10 and then from the 13-km RAP (B16) starting in 2011 (Table 2). The FAA, recognizing the potential value of frequent CAM simulations for anticipating the occurrence, timing, and three-dimensional coverage of convective storms for flight-planning guidance, provided significant support for the required computing infrastructure in the mid- to late 2000s. Successful
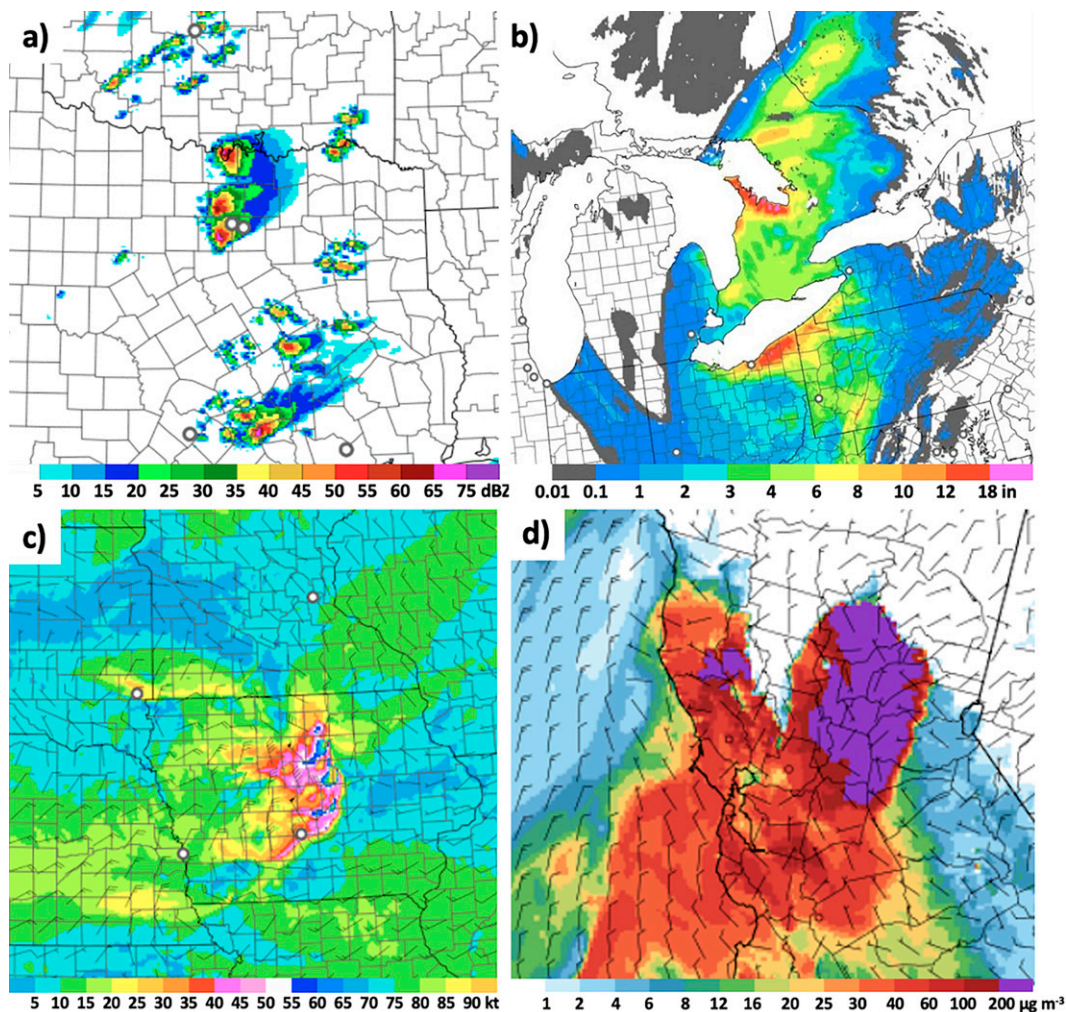
FIG. 1. Example HRRR forecasts for high-impact weather events: (a) evening supercells including an EF3 tornado producer impacting Dallas, TX [4-h simulated composite radar reflectivity forecast (dBZ) valid at 0100 UTC 21 Oct 2019]; (b) lake-effect snowstorm near Lakes Huron and Erie [17-h variable density accumulated snow depth (in.) valid at 2300 UTC 1 Dec 2020]; (c) 80-m wind speed (kt) during Iowa derecho (13-h forecast valid at 1700 UTC 10 Aug 2020); and (d) dense smoke pollution [PM2.5 concentrations (μg m^{-3})] from Camp Fire in California (24-h forecast valid at 0000 UTC 11 Nov 2018).

demonstrations of the experimental HRRR system in the subsequent several years (e.g., Smith et al. 2008) spurred the development of the Consolidated Storm Prediction for Aviation (CoSPA) forecast product (Wolfson et al. 2008). Used for strategic flight planning, CoSPA provides 0–8-h forecasts of vertically integrated liquid (VIL) and echo tops (ET) by blending these products from the Corridor Integrated Weather System (CIWS; Klingle-Wilson and Evans 2005) with HRRR forecasts.

Beyond the aviation applications of the HRRR, the severe-weather forecasting community, most notably the National Weather Service's Storm Prediction Center (SPC), recognized the utility of CAM guidance for predicting the mode of potentially severe convection to aid in the development of severe weather outlooks (e.g., Kain et al. 2006; Clark et al. 2012). The availability of hourly updated CAM forecasts with 3-km

grid spacing has advanced the state of the science towards the "Warn-on-Forecast" (WoF) paradigm (Stensrud et al. 2009), in which severe weather warnings could be issued based upon NWP. More recently, other applications of HRRR forecasts have emerged. Notable among these has been renewable energy, in which forecasts of turbine hub-height winds and solar irradiances are important for anticipating variable electricity supply in regions where these renewable resources are available (Marquis et al. 2011; James et al 2017). An additional major application of HRRR forecasts has been for hydrology and flood forecasting, with HRRR output (especially precipitation) providing input to the operational National Water Model since 2016 (e.g., Lahmers et al. 2019). HRRR analyses and forecasts are also widely used for research, education, and commercial applications. Research ranges from very-high-resolution simulation, with

TABLE 2. History of experimental and operational HRRR versions.

HRRR version	Domain(s)	Notes (major changes for DA and model, dates)
2008 experimental	Northeast corridor United States (745 × 383 grid points)	Real-time forecasts starting in September 2007; initial conditions from RUC using radar-based latent-heating assimilation (Weygandt et al. 2022)
2009 experimental	Eastern 2/3 CONUS (1000 × 700 grid points)	Expanded domain
2010 experimental	CONUS (1800 × 1060 grid points)	Expanded domain to CONUS; forecast period extended from 12 to 15 h
2011 experimental	CONUS	Initial conditions from RAP starting in 2011, including 13-km land surface fields
2012 experimental	CONUS	DA: Improved timing of convection initiation and reduced false alarms through changes to RAP surface data assimilation and cloud analysis
2013 experimental	CONUS	DA: Change from 3DVar to hybrid ensemble-variational DA in RAP; introduction of 1-h HRRR spinup with reflectivity DA, 3-km 3DVar analysis, and 3-km cloud analysis. Model: change from MYJ to MYNN PBL scheme
HRRRv1 (2014 experimental)	CONUS	DA: Change from 3DVar to hybrid ensemble–variational DA in HRRR; operational 30 Sep 2014
HRRRv2 (2015–16 experimental)	CONUS	Model: Reduced biases in parameterizations; initial RH-based SGS clouds; reduced wilting point; aerosol-aware precipitation microphysics; introduction of full cycling of 3-km land surface fields; forecast period extended to 18 (36) h in operational (experimental) version. DA: PBL pseudo-innovations added; lightning DA added to 1-h HRRR spinup; operational 23 Aug 2016
HRRRv3 (2016–17 experimental)	CONUS, Alaska	Model: Improvements in MYNN PBL scheme (addition of mass-flux scheme, transition to EDMF framework); hybrid vertical coordinate. DA: improvements to better retain stratiform clouds; reduced latent heating for radar in RAP; Alaska domain coverage; operational 12 Jul 2018
HRRRv4 (2018–20 experimental)	CONUS, Alaska	DA (CONUS domain): Use of 36-member HRRRDAS ensemble information for initial conditions. Model: MYNN PBL improvements for better representation of SGS clouds; specification of Great Lakes temperature and ice coverage based on FVCOM; introduction of small-lake model and wildfire smoke forecasting capability; removal of microphysics temperature-tendency limit; operational 2 Dec 2020

HRRR data providing initial and boundary conditions, to machine-learning applications (e.g., Arulaj and Barros 2021; Wang et al. 2022).

Throughout the history of the HRRR system, valuable assessment of forecasts has come from field projects (e.g., Olson et al. 2019a) and annual testbeds focused on severe thunderstorms, quantitative precipitation forecasting, convective storm impacts on aviation, and winter weather (Clark et al. 2012; Erickson et al. 2019). Individual forecasters have contributed to HRRR development through assessment of regional forecast performance. The forecast deficiencies that were identified motivated testing of possible system changes, first for individual cases, and then for long retrospective periods with verification. Decisions on proposed system changes

relied extensively on the forecast performance measures described by James et al. (2022), with emphasis on the measures related to convective-storm forecasting, renewable energy, and hydrology.

The HRRR was built with community-developed model and DA tools: a customized version of the Advanced Research version of the Weather Research and Forecasting (WRF-ARW) Model (Skamarock et al. 2019; Powers et al. 2017) and the Gridpoint Statistical Interpolation (GSI) analysis system (Wu et al. 2002; Whitaker et al. 2008; Kleist et al. 2009). Use of community-supported software for an operational model facilitates collaboration on system development, allowing the operational and research communities to work jointly toward the advancement of NWP capabilities and

TABLE 3. History of RAP and HRRR versions at GSL and operational implementations at NCEP. The computing resources required for the operational HRRR are expressed in terms of peak usage (high-water mark).

RAP (13 km) version/ HRRR (3 km) version	Version finalized at GSL—Experimental	Implementation at NCEP—Operational	Operational HRRR computing resources (max instantaneous node usage)
RAPv1	19 Mar 2012	1 May 2012	
RAPv2	17 Mar 2013	25 Feb 2014	
HRRRv1	10 Apr 2014	30 Sep 2014	124 nodes on WCOSS phase 1
RAPv3/HRRRv2	10 Apr 2015	23 Aug 2016	124 nodes on WCOSS phase 2
RAPv4/HRRRv3	26 May 2017	12 Jul 2018	260 nodes on WCOSS Cray
RAPv5/HRRRv4	5 Jun 2019	2 Dec 2020	491 nodes on WCOSS Cray

increasing the efficiency of transitions to operations (e.g., Bernardet et al. 2008).

On 30 September 2014, the first NWS-operational version of the HRRR (HRRRv1; Table 3), covering the entire CONUS (Fig. 2), was implemented by NCEP Central Operations (NCO), with nearly 100% operational reliability and widespread product availability and use. Downstream forecast products developed for the NWS also relied extensively on the HRRR, including its cloud fields for the Localized Aviation Model Output Statistics Program (LAMP; Glahn et al. 2017), its near-surface fields for the Real-Time Mesoscale Analysis (RTMA; De Pondeca et al. 2011), all fields for the National Blend of Models (NBM; Hamill et al. 2017), and its precipitation forecasts for the NOAA National Water Model (https://water.noaa.gov/about/nwm). In addition to providing hourly forecasts out to 15 h (HRRRv1) and 18 h (later versions), a longer forecast every 6 h was added to HRRRv3 (out to 36 h) and HRRRv4 (out to 48 h; Table 4). The longer forecasts are helpful for preparing day 2 outlooks (e.g., for severe weather forecasting) and for covering weather events that span multiple days. The availability of increased computing resources at NCEP (Table 3) enabled the longer forecasts in HRRRv3–v4 and the addition of the ensemble

FIG. 2. HRRR domains (green): HRRR CONUS (v1, v2, v3, and v4), and Alaska (v3 and v4). Also shown is the 13-km RAP domain (white).

component to HRRRv4. An Alaska domain (Fig. 2) was added with HRRRv3 in 2018. The availability of operational HRRR forecasts has led to significant, quantifiable economic savings through better decision making for activities such as wind-energy production, commuting, and agriculture (Turner et al. 2022, Hartman et al. 2021).

The HRRRv4 represents the final operational WRF-ARW-based CAM implementation at NCEP. Work is now underway to transition the hourly updating CAM capability represented by the HRRR system into a framework built around NOAA's Unified Forecast System (UFS). The operational HRRR is tentatively scheduled for replacement by a Rapid Refresh Forecast System (RRFS) in 2024. The operational HRRR represents an important baseline for forecast performance for the RRFS while it is being developed.

The purpose of this article, the first of a two-part series, is to summarize the design of the HRRR system. The following section provides a description of its prognostic variables and physical parameterization schemes. Section 3 provides a detailed description of the HRRR initialization. Section 4 provides case study examples illustrating qualitative HRRR forecast performance for high-impact weather phenomena. The conclusion (section 5) includes a discussion of future CAM development in the era succeeding the HRRR. The appendix contains a list of acronyms used in this paper and their definitions. The second paper (James et al. 2022) in this two-part series documents HRRR objective forecast performance.

2. WRF Model configuration for HRRR

The HRRR, like the RAP, uses the non-hydrostatic WRF-ARW dynamic core with a set of dynamic options and physical parameterizations described in this section. Wide community testing and development of the WRF Model (Powers et al. 2017; with several common coauthors included on this paper) was essential to HRRR development and operational implementation. Within the WRF-ARW framework, HRRR configurations (Table 4) have generally used the same dynamics and physics options as the RAP (Table 2 of B16); a notable exception is that the HRRR, with 3-km grid spacing sufficient to produce explicit convective storms, does not use a convective parameterization. Additional unique features of the HRRR dynamics and physics options as compared to the RAP are described below.
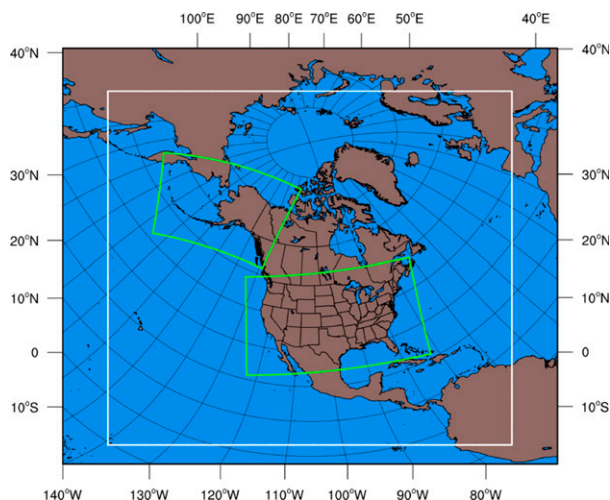
TABLE 4. Model and physics configuration for HRRRv1–HRRRv4.

System	HRRRv1	HRRRv2	HRRRv3	HRRRv4
Model	WRF-ARWv3.4.1+	WRF-ARWv3.6+	WRF-ARWv3.8.1+	WRF-ARWv3.9.1+
Domain	CONUS	CONUS	CONUS, Alaska	CONUS, Alaska
Initialization frequency	1 h	1 h	1 h, 3 h	1, 3 h
Map projection	Lambert conformal	Lambert conformal	Lambert conformal (CONUS), polar stereographic (AK)	Lambert conformal (CONUS), polar stereographic (AK)
Grid points (x, y)	1800×1060	1800×1060	1800×1060, 1300×920	1800×1060, 1300×920
Grid spacing	3 km	3 km	3 km	3 km
Vertical layers	51	51	51	51
Pressure top	20 hPa	20 hPa	20 hPa	15 hPa
Lateral boundary conditions	RAP	RAP	RAP	RAP
Initial conditions	RAP post-DFI plus 1-h spinup, 3-km GSI with GDAS	RAP post-DFI plus 1-h spinup, 3-km GSI with GDAS	RAP post-DFI plus 1-h spinup, 3-km GSI with GDAS	HRRRDAS mean plus 1-h spinup, 3-km GSI with HRRRDAS
Vertical coordinate	Sigma	Sigma	Hybrid sigma-terrain-following	Hybrid sigma-terrain-following
Horizontal/ vertical advection	Fifth-order upwind	Fifth-order upwind	Fifth-order upwind	Fifth-order upwind + IEVA
Scalar advection	Positive definite	Positive definite	Positive definite	Positive definite
Large time step	20 s	20 s	20 s	20 s
Upper-level damping	Rayleigh, dampcoef = 0.2 s^{-1}, zdamp = 5000 m	Rayleigh, dampcoef = 0.2 s^{-1}, zdamp = 5000 m	Rayleigh, dampcoef = 0.2 s^{-1}, zdamp = 5000 m	Rayleigh, dampcoef = 0.2 s^{-1}, zdamp = 5000 m
Computational horizontal diffusion	None	Sixth-order (0.25)	Sixth-order (0.25), horizontal only (not on slopes), applied to all variables	Sixth-order reduced to 0.04 for tracers, including water vapor and hydrometeors, and to 0.12 for other model variables
Forecast frequency	Hourly	Hourly	Hourly, 3 h	Hourly, 3 h
Forecast duration	15 h	18 h	36 h every 6 h, otherwise, 18 h	48 h every 6 h, otherwise, 18 h
Radiation	RRTMG	RRTMG	RRTMG	RRTMG (modified with SGS cloud)
Land surface, including No. of layers	RUC LSM, nine soil levels, two-layer snow (v3.5+)	RUC LSM, nine soil levels, two-layer snow, reduced wilting point (v3.6+)	RUC LSM, nine soil levels, two-layer snow (v3.8+)	RUC LSM, nine soil levels, two-layer snow (v3.9+)
Land use	30″ MODIS	30″ MODIS	30″ MODIS,	15″ MODIS, BNU soil type (via WRF), switch to MODIS albedo
Planetary boundary and surface layer	Mellor–Yamada–Nakanishi–Niino (v3.5+)	Mellor–Yamada–Nakanishi–Niino (v3.6+)	Mellor–Yamada–Nakanishi–Niino (v3.8+)	Mellor–Yamada–Nakanishi–Niino (v3.9+)
Subgrid-scale clouds	None	MYNN RH-based (Benjamin et al 2016, their appendix B)	MYNN prognostic SGS cloud fraction, cloud water	MYNN removed limit to SGS cloud water, reduced radii
Orographic drag	None	None	Small-scale orographic drag	Turbulent drag from subgrid orography (CONUS only)
Cloud Microphysics	Thompson (v3.4.1)	Thompson–Eidhammer "aerosol-aware" (v3.6.1)	Thompson–Eidhammer "aerosol-aware" (v3.8)	Thompson–Eidhammer "aerosol-aware" (v3.8)
Microphysics temperature tendency limit	0.07 K s^{-1}	0.07 K s^{-1}	0.07 K s^{-1}	None needed due to IEVA

a. Dynamics

While it is generally accepted that deep, moist convection is not truly "resolved" at horizontal grid spacings of greater than 1 km (Bryan et al. 2003), NWP forecasts with explicit convection at grid spacings of 2–4 km have nevertheless been shown to provide significant skill improvements over those with grid spacings greater than 5 km (Weisman et al. 1997). A horizontal grid spacing of 3 km was chosen for the HRRR system, striking a balance between increasing computational cost with higher resolution and the benefits of finer representation of convective storms (Schwartz and Sobash 2019), coastlines, and terrain (Olson et al. 2019a). Considering possible applications in future operational CAMs such as the RRFS and WoF System, we have during the past few years produced experimental forecasts, initialized from HRRR analyses, over sub-CONUS domains with horizontal grid spacing ~1 km. These experimental higher resolution forecasts have focused on wind (Olson et al. 2019a) and precipitation (English et al. 2021) in complex terrain, coastal clouds and fog, lake-effect snow, supercooled liquid water for in-flight icing hazards, and convective storms. Olson et al. (2019a) noted improvements in wind forecasts with higher resolution; investigations of the results for other high-resolution forecast applications are ongoing.

The HRRR uses the same specification of 51 vertical levels[1] as the RAP (Table 7 in B16). The lowest model level is at ~8 m AGL for areas near sea level, and somewhat closer to the ground in higher terrain. The vertical spacing between vertical levels increases from approximately 15–30 m in the lowest levels to about 400 m in the midtroposphere and increases again up to about 700 m near the tropopause. In RAPv4 and HRRRv3, a hybrid pressure-sigma vertical coordinate (Klemp 2011) was introduced, replacing the pure sigma coordinate in HRRRv1–v2. The new vertical coordinate transitions from the terrain-following sigma coordinate near the surface to isobaric at mid and upper levels and allows for a reduction of small-scale numerical noise aloft in situations of flow across mountain barriers (Kim et al 2019). Beck et al. (2020) demonstrated the benefits of the change in vertical coordinate for both the RAP and the HRRR.

The time step used for the HRRR is 20 s (Table 4), slightly above the recommended 18 s for a 3-km grid length [Skamarock et al 2019; section 3c(1)], an important extension considering limited operational computational resources. This extension was enabled by limiting the cloud-physics temperature tendency to 0.07 K s^{-1} in HRRRv1–v3. However, the advent of the new implicit-explicit vertical advection option for WRF-ARW (Wicker and Skamarock 2020) allowed for removal of the temperature tendency limit in HRRRv4. Differences between HRRR forecasts with and without the temperature-tendency limit are particularly noticeable for the maximum vertical velocities in convective-storm

___

[1] The target for the future RRFS is 65 vertical levels, with improved resolution in and near the PBL (enabling better representations of clouds and temperature inversions) and a higher model top (enabling more effective satellite-radiance data assimilation).

updrafts. Whereas maximum updraft speeds plateaued around 30 m s^{-1} in HRRRv1–v3 forecasts, the updraft speeds in HRRRv4 forecasts are more realistic, at times exceeding 60 m s^{-1} (not shown).

The mean terrain elevation for each 3-km grid area in the HRRR CONUS and Alaska domains was specified using the WRF Preprocessing System (WPS; Skamarock et al. 2019) based on 30-arc-s USGS 2010 Global Multi-resolution Terrain Elevation Data. Terrain modification was needed in the Alaska domain to avoid CFL instability in strong flow. Following the WPS interpolation, a nine-point smoother was applied to the gridded terrain elevation in the Alaska domain at all points higher than 2500 m MSL, reducing the maximum gradient from 29.1° to 21.8° and thus improving model stability.

To ensure damping of poorly resolved features having a length scale 2–4 times the model grid spacing, the HRRRv2 employed sixth-order horizontal diffusion within WRF (Xue 2000; Knievel et al. 2007). A diffusion parameter modulates the magnitude of the reduction in strength of features of scale twice the grid interval; this parameter was set to 0.25 for HRRRv2 and HRRRv3 (Table 4). Beginning with HRRRv3, the sixth-order diffusion was modified to account for local terrain slope, which acted to reduce inadvertent vertical mixing along complex or sloping terrain (Arthur et al. 2021). For HRRRv4, the diffusion parameter was decreased substantially, to 0.04 for water vapor and hydrometeors and to 0.12 for other variables.

b. Atmospheric model physics

A major focus of physics development over the past few years has been the improved treatment of subgrid-scale (SGS, i.e., sub-3-km horizontal dimension for HRRR) clouds and the turbulence within cloudy and clear environments (Table 4). The RAP-HRRR physics suite accounts for both stratus and shallow-cumulus SGS clouds within the Mellor–Yamada–Nakanishi–Niino eddy-diffusivity/mass-flux (MYNN-EDMF; Nakanishi and Niino 2009; Olson et al. 2019b) planetary boundary layer scheme using the Chaboureau and Bechtold (2002, 2005) approach, while the associated nonlocal transport is parameterized by a multi-plume mass-flux scheme following Neggers (2015). With HRRRv1, SGS cloud fraction was determined based on Xu and Randall (1996) using grid-scale RH, but starting with HRRRv2, the cloud fractions and associated SGS cloud mixing ratios are determined within the MYNN-EDMF, where they directly impact the turbulence. The shortwave and longwave radiation physics, RRTMG (Iacono et al. 2008), uses the SGS cloud properties (from MYNN-EDMF) in its calculations. The effective radii for the SGS clouds starting with HRRRv4 are determined based on Miles et al. (2000), Turner et al. (2007), and Mishra et al. (2014). A more detailed discussion of MYNN-EDMF boundary layer scheme development and coupling to other model components is provided by Olson et al. (2019b). As a result of combined physics changes, particularly in the representation of SGS, HRRRv4 has reduced bias errors in surface

temperature and incoming shortwave radiation relative to previous HRRR versions (James et al. 2022).

The parameterization of the wind drag force imparted by subgrid topography down to ~1 km in horizontal extent was implemented in HRRRv4. Small-scale orographic gravity wave drag due to wave breaking that can occur within and immediately above stable PBLs is represented by the parameterization of Tsiringakis et al. (2017), which was implemented in HRRRv3. The HRRRv4 adds the parameterization of Beljaars et al. (2004), which represents turbulent form drag imparted by subgrid topography.[2] These two schemes represent drag forces missing from the resolved gridscale dynamics. Tests for retrospective periods in all four seasons demonstrated that the schemes reduced high wind speed biases of modeled near-surface winds.

The HRRR uses the Thompson bulk scheme (Thompson et al. 2004, 2008; Thompson and Eidhammer 2014) to represent cloud microphysics. The capabilities of this scheme increased during the HRRR era, and as of HRRRv4 it included one-moment prediction of snow and two-moment prediction of cloud water, cloud ice, rain, and graupel/hail. Beginning with HRRRv2, the scheme incorporated "aerosol awareness"; climatological water-friendly and ice-friendly 3D aerosol concentrations are prescribed in the initial conditions of each HRRR simulation. During the model integration, aerosols affect cloud droplet nucleation and ice activation, and processes such as aerosol collection by precipitation are also represented. Starting with HRRRv3, the RRTMG scheme included the impacts of the aerosols on shortwave and longwave radiation as well.

c. Land surface physics

Like the RAP, the HRRR uses the RUC land surface model (LSM), originally developed for use in the RUC system (Smirnova et al. 2000, 2016) and often applied as an LSM option by WRF users. The RUC LSM receives surface exchange coefficients as input from the MYNN surface layer scheme (Olson et al. 2021) and uses them in an iterative algorithm to solve for the surface energy balance. In 2013, the soil modeling expanded from six levels to nine levels, better representing soil conditions at the interface with the atmosphere and improving the 2-m temperature diurnal cycle (e.g., Fig. 2 in Smirnova et al 2016). HRRR versions 2–4, with continuously cycled land surface variables, are able to represent seasonal snowfall accumulation, and previous work (Rasmussen et al. 2011) suggests that the HRRR has fine enough grid spacing to do so realistically. Updates to the RUC LSM starting with HRRRv2 included improved treatment of snow melting, trimming, and building (Smirnova et al. 2016). Additional improvements within the scheme have included its application in conditions of sea ice, an accounting for subgrid heterogeneity in land surface characteristics, a simple irrigation scheme, and a seasonal variation of roughness length for croplands.

Starting with HRRRv3, a snow "mosaic" approach for grid cells with partial snow cover, utilizing a separate treatment of snow-covered and snow-free portions of the grid cells, has been implemented. Also, an empirical formulation is used in the RUC LSM to evaluate the density of solid precipitation based on snow, ice, and graupel fall rates predicted by the Thompson microphysics scheme for improved prediction of accumulated snowfall.
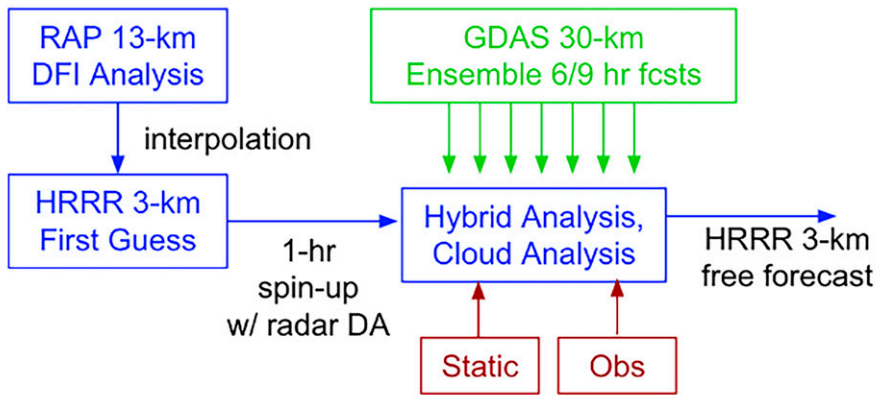
d. Aerosol and smoke prediction

A basic wildfire smoke forecasting capability has been incorporated in the RAPv5 and HRRRv4 systems (Ahmadov et al. 2017). This addition has proved to be a critical tool for air quality and visibility forecasting applications. The RAP and HRRR employ a single tracer, representing particulate matter less than 2.5 μm (PM2.5), to forecast smoke within the modeling systems. Smoke sources are initialized from satellite-based fire radiative power observations. The evolution of the smoke is treated with a simplified version of WRF-Chem (Grell et al. 2005). The HRRR is configured to use boundary conditions of smoke from the RAP, which allows smoke from outside the CONUS domain (particularly from Canada and Mexico) to influence air quality within the CONUS domain (Wang et al. 2010; Wu et al. 2018). The HRRR also continuously cycles smoke; therefore, each hourly HRRR run begins with a 3D smoke field derived from the previous run's 1-h forecast. The HRRR employs simple direct radiative feedback of the smoke on atmospheric evolution, allowing incoming solar radiation to be attenuated by thick smoke plumes, and also represents precipitation scavenging of smoke.
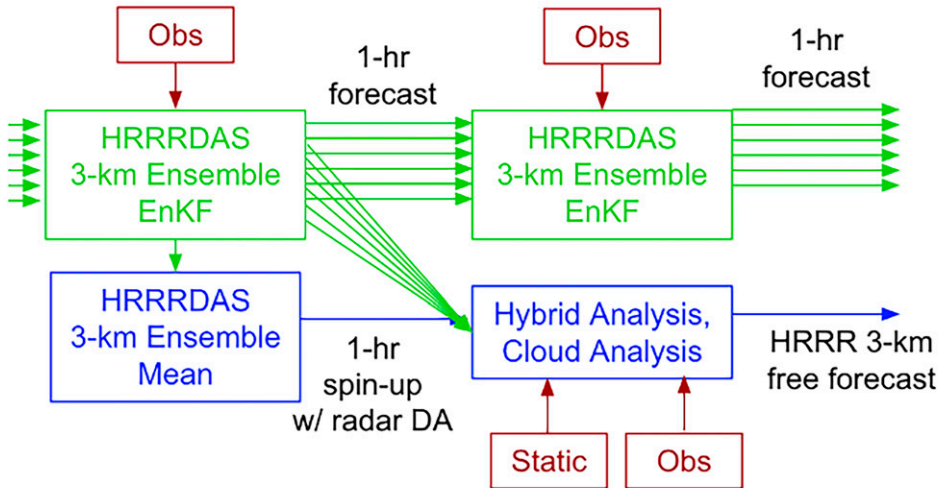
3. Model initialization

In this section, we describe the components of the HRRR initialization, including system flow charts, observations assimilated, GSI variational and ensemble algorithms, cloud-hydrometeor assimilation, land surface assimilation, and smoke initialization. The initialization steps common to all HRRR versions (Figs. 3a,b) are a first guess, a 1-h "pre-forecast," and a GSI analysis. For HRRRv1-v3, a downscaled RAP analysis provided the first guess, and the 80-member Global Data Assimilation System (GDAS) in the Global Forecast System (Kleist and Ide 2015) provided the background error covariances for the GSI hybrid ensemble-variational data assimilation (Fig. 3a). A major change in HRRRv4 for the CONUS domain was to add an hourly cycled, 36-member, convection-allowing WRF ensemble to the system (section 3d; Dowell et al. 2016). This ensemble was named the HRRR Data Assimilation System (HRRRDAS), analogous to the GDAS. For HRRRv4 CONUS initialization, the HRRRDAS analysis mean provides the first guess, and the HRRRDAS member 1-h forecasts provide the background error covariances for the GSI hybrid data assimilation (Fig. 3b). The Alaska domain in HRRRv4 continues to be initialized as in HRRRv3, with a first guess from the RAP and background error covariances from the GDAS.

---

[2] Due to an oversight on the need to update static files, the Alaska domain of HRRRv4 does not use this Beljaars et al. (2004) parameterization.

a) Phase One (HRRRv1-v3)

RAP 13-km DFI Analysis

interpolation

HRRR 3-km First Guess

GDAS 30-km Ensemble 6/9 hr fcsts

1-hr spin-up w/ radar DA

Hybrid Analysis, Cloud Analysis

HRRR 3-km free forecast

Static

Obs

b) Phase Two (HRRRv4)

Obs

HRRRDAS 3-km Ensemble EnKF

1-hr forecast

Obs

HRRRDAS 3-km Ensemble EnKF

1-hr forecast

HRRRDAS 3-km Ensemble Mean

1-hr spin-up w/ radar DA

Hybrid Analysis, Cloud Analysis

HRRR 3-km free forecast

Static

Obs

c) Phase Three (RRFS)

Obs

RRFSDAS 3-km Ensemble EnKF

1-hr forecast

Obs

RRFSDAS 3-km Ensemble EnKF

1-hr forecast

recentering

recentering

RRFS 3-km Control Hybrid Analysis

1-hr forecast

RRFS 3-km Control Hybrid Analysis

1-hr forecast

RRFS 3-km control free forecast

RRFS 3-km control free forecast

Static

Obs

Static

Obs

FIG. 3. Wiring diagrams for hourly initialization of (a) HRRRv1–v3, (b) HRRRv4, and (c) the planned RRFS. Blue, green, and red indicate deterministic, ensemble, and other information (observations and static covariances), respectively.

a. Observations

The HRRR uses the same broad set of observations as the RAP (B16, section 2a), except satellite radiance observations are not assimilated in the CONUS domain. New to RAPv5 and HRRRv4 is the assimilation of "TCVitals" tropical cyclone minimum pressure and location (Trahan and Sparling 2012). Unique aspects of how some observation types are assimilated, including radar reflectivity, Vaisala lightning, METAR cloud-ceiling height and visibility, and satellite cloud-top pressure, are described in upcoming subsections. The use of surface observations in the HRRR, including vertically projected PBL "pseudo-innovations" (B16, section 2f), is important for the accuracy of short-range predictions of PBL evolution.

The HRRR observation assimilation window, observation errors, and model surface vs. station elevation adjustment for assimilation of surface observations are like those in the RAP (B16, section 2a). Even with relatively fine 3-km grid length, 6% of METAR and mesonet stations have elevation differences from HRRR topography exceeding 100 m, which would result in a 1-K daytime bias without this adjustment.

b. GSI

Community-supported GSI software, with unique extensions for the HRRR application, provides the framework for the HRRR data assimilation. The HRRR performs a 3D hybrid ensemble–variational (EnVar) analysis every hour, with background error covariances from a combination of static and ensemble-based covariances. The unique extensions of GSI for HRRR include a utility to convert 3D radar-reflectivity and lightning observations to a 3D distribution of latent heating (Weygandt et al. 2022), the stratiform cloud-hydrometeor data assimilation (SCHDA; Benjamin et al. 2021a), and soil adjustment based on near-surface temperature and water vapor analysis increments, as described below in sections 3c, 3e, and 3f.

c. Radar and lightning assimilation and the EnVar analysis

The 13-km RAP (B16; Hu et al. 2017; Lin et al. 2017; Benjamin et al. 2021a; Weygandt et al. 2022) is the parent model of the HRRR, providing both initial and boundary conditions. The RAP cycle initialized three hours prior to the HRRR initialization provides lateral boundary conditions to the HRRR at 3-h intervals.

For HRRRv1-v3, a first-guess state at $T - 1$ h comes from interpolating the 13-km RAP post-DFI analysis to the 3-km HRRR grid (Fig. 3a; Weygandt et al. 2022). In HRRRv4 (Fig. 3b), the 36-member HRRRDAS analysis ensemble mean is used instead as the first-guess state at $T - 1$ h. In all HRRR versions, the first guess contains mesoscale circulations established during the hourly cycling with conventional and radar-data assimilation in the parent system (RAP or HRRRDAS). Since the first guess comes from either the 13-km RAP (HRRRv1-v3) or an ensemble mean (HRRRv4), this first guess is not "spun up" on the smallest resolvable scales on the HRRR grid.

The first guess at $T - 1$ h is the starting point for a HRRR "pre-forecast" integrated from $T - 1$ h to $T - 0$ h, during which rapid energy growth occurs for small-scale features (Skamarock 2004) including convective storms. The execution of the 1-h pre-forecast is carried out with latent heating based on 3D MRMS radar data, augmented with lightning data. Radar and lightning data at four times (i.e., at 15-min intervals) are used, coarsely representing evolution during the 1-h period (Weygandt et al. 2022).

After the pre-forecast, the HRRR assimilates conventional observations with GSI's hybrid 3DEnVar method, leveraging a combination of static and flow-dependent, ensemble-based background error covariances (Figs. 3a,b). The HRRR DA is configured similarly to the RAP DA (B16; Hu et al. 2017), leveraging all the conventional observations used in the RAP except satellite radiances over CONUS. In HRRRv1-v3, the background ensemble fields from the 80-member GDAS (horizontal grid spacing approximately 25 km) are interpolated to a 12-km analysis grid. In the hybrid DA in HRRRv4, the HRRRDAS background ensemble is used at its native 3-km grid spacing. Additional details of the HRRRv4 initialization are in Table 5. Positive impacts of the assimilation of conventional observations (rawinsonde, aircraft, surface, etc.) on forecast skill have been shown to persist through at least 12 h for the RAP (James and Benjamin 2017). Within the 3-km GSI at $T - 0$ h, the SCHDA (section 3e) is also applied.

d. 3-km ensemble data assimilation for HRRRv4 using the HRRRDAS

Convection-allowing ensemble systems have recently been developed both for research use (e.g., Schwartz et al. 2021) and operational deployment (e.g., Hagelin et al. 2017). Such ensembles represent uncertainty both in initial conditions and in model physics, and they allow the use of high-resolution, flow-dependent covariances to improve data assimilation. HRRRv4 features a significant data-assimilation advancement over previous versions by using the 36-member, hourly cycled, 3-km HRRRDAS rather than the coarser global GDAS for the hybrid data assimilation (Figs. 3a,b). This design enables more accurate and balanced spreading of observation information in regions of complex flow and within the PBL.

The HRRRDAS initialization is staggered, with 18 members initialized daily at 0900 UTC and 18 members initialized daily at 2100 UTC. Each member is cycled hourly for 24 h before being replaced; thus, 36 ensemble members are available at each hour of the day. The atmospheric state in each HRRRDAS member is initialized by adding a perturbation from a corresponding member in the 9-h GDAS ensemble forecast to the RAP analysis at 0900/2100 UTC. This strategy allows the HRRRDAS to take advantage of recent global atmospheric information in two ways: the GFS state inherited through the twice-daily RAP partial cycles (B16; James and Benjamin 2017) and perturbations in the GDAS. The land surface state in each HRRRDAS member is reinitialized daily from the 1-h HRRR forecast valid at 0900/2100 UTC.

TABLE 5. Summary of assimilation of conventional (B16, section 2a) and MRMS radar-reflectivity (Smith et al. 2016) observations in the 36-member HRRRDAS and deterministic HRRRv4.

Parameter	HRRRDAS (3-km CONUS domain)	HRRRv4
Assimilation method: Conventional observations	EnKF	CONUS 3D EnVar: 85% weight to BEC from HRRRDAS 1-h forecast, 15% weight to static BEC Alaska 3D EnVar: 85% weight to BEC from GDAS forecast, 15% weight to static BEC
Localization full width: Conventional observations	Horizontal: 300 km Vertical: 0.5 scale height	Horizontal: 110 km Vertical: 3 grid levels
WRF model variables updated from conventional observations	Zonal and meridional wind components; potential temperature; water vapor and cloud water mixing ratios	Zonal and meridional wind components; potential temperature; pressure; water vapor mixing ratio
MRMS reflectivity observation preprocessing	Horizontal thinning to 6-km (12-km) spacing in precipitation (non-precipitation) regions; vertical thinning also applied	Interpolation to model grid points
Assimilation method: Radar-reflectivity observations	EnKF	Diabatic initialization and stratiform cloud-hydrometeor data assimilation (SCHDA)
Localization full width: Radar-reflectivity observations	Horizontal: 18 km Vertical: 0.5 scale height	
WRF model variables updated from radar-reflectivity observations	Zonal and meridional wind components; potential temperature; water vapor, cloud water, rain, snow, and graupel mixing ratios	All variables affected by diabatic initialization. Following variables updated by SCHDA: potential temperature; water vapor, cloud water, rain, and snow mixing ratios

Ensemble spread in the HRRRDAS comes from multiple sources: initial-condition perturbations from the GDAS; random, spatially correlated boundary condition perturbations (Torn et al. 2006, Romine et al. 2014); and hourly posterior relaxation-to-prior spread (Whitaker and Hamill 2012, Schwartz and Liu 2014). The HRRRDAS uses an ensemble Kalman filter (EnKF; Houtekamer and Zhang 2016), specifically the ensemble square-root filter (EnSRF; Tippett et al. 2003) to assimilate conventional and radar-reflectivity observations (Table 5). To prevent development of excessive cloudiness during cycling, hourly cloud clearing is also applied to members individually, employing the same non-variational cloud-clearing method as in the HRRR (Benjamin et al. 2021a).

Although the operational implementation of a convection-allowing ensemble and use for data assimilation represent significant advances, we consider the HRRRv4 configuration to be an intermediate phase (Fig. 3b) toward the proposed next-generation NOAA regional modeling system, the RRFS. In one RRFS design being considered, a continuously cycled deterministic control member would be two-way coupled with a continuously cycled ensemble (Fig. 3c); this design is similar to that of the NOAA GFS (Wang et al. 2013). This proposed future configuration would improve upon the HRRRv4 configuration by adding hourly cycling of the deterministic control member and eliminating the use of the ensemble mean in initializing the control member. Research will be needed to optimize storm-scale data assimilation (e.g., Wang and Wang 2021) and to harmonize regional and global ensemble modeling (e.g., Schwartz et al. 2021).

e. Cloud and hydrometeor assimilation

The SCHDA procedure (Benjamin et al. 2021a) procedure is a non-variational method to initialize stratiform clouds in the RAP and HRRR, applied after the EnVar assimilation of conventional observations. Clouds in the model background are updated with observations of cloud layers (or their absence) from METAR ceilometer/visibility and satellite cloud-top observations. The SCHDA procedure is effective for initializing stratiform clouds and retaining cloud layers in the model forecast, which is particularly important for aviation applications and PBL evolution. SCHDA consists of both cloud clearing and cloud building. In volumes with building or clearing, temperature and water vapor are modified to ensure convective stability and to produce realistic vertical profiles. As described by Benjamin et al. (2021a), precipitation hydrometeors (rain and snow mixing ratios) are added, based on radar-reflectivity observations, in limited circumstances.

f. Land surface assimilation

Under the assumption that near-surface atmospheric forecast errors may be related to errors in the soil state, the HRRR adjusts soil temperature and moisture with equations that depend on the EnVar analysis increments in temperature and relative humidity at the lowest model level in the atmosphere (B16, their appendix B; Smirnova et al 2016; Benjamin et al. 2022b). To retain high-resolution soil information, including snow, HRRRv2 and later versions have continuously cycled land surface variables between model initializations.

In HRRRv3-v4, satellite-detected greenness vegetation fraction (GVF) from the polar-orbiting Visible Infrared Imaging Radiometer Suite (VIIRS) instrument is used to update vegetation greenness daily instead of using climatological values. This information is used to partition each grid cell into vegetated and bare soil components. The use of this remotely sensed land surface dataset enables a more realistic evolution of surface fluxes within the RUC LSM system, particularly during anomalously dry or wet periods.

All HRRR versions include daily specifications of sea surface temperature (SST) and snow cover. The updates for these variables are nominally valid for 0000 UTC each day, when new data from a daily analysis become available. The SST data are provided by the Real-Time Global (RTG) analysis developed by NCEP (updated to an SST analysis within the GDAS in February 2020), and snow cover information is provided by NOAA's daily Interactive Multisensor Snow and Ice Mapping System analysis at 4-km grid spacing (Helfrich et al. 2007).

In HRRRv4, lake temperatures are specified more accurately, including loose coupling with the NOAA Great Lakes Operational Forecast System (Anderson et al. 2018, Benjamin et al. 2022a) based on the FVCOM (Chen et al. 2006) to provide improved initial conditions in those regions. Variables copied directly from the interpolated FVCOM grid to the HRRR grid include lake surface temperatures and fractional lake ice coverage. Use of FVCOM forecast fields allows the HRRR to better estimate Great Lakes surface conditions, particularly in winter when information on fractional ice improves predictions of surface fluxes or at times when clouds obscure the Great Lakes for many consecutive days and render satellite-based estimates less useful (Fujisaki-Manome et al. 2020). HRRRv4 predicts the evolution of other lakes using the 10-level lake model component of the Community Land Model (CLMv4.5; Oleson et al. 2010; Zeng et al. 2002). Continuous HRRR cycling of 3D lake variables over many months allows a more realistic lake temperature initialization than from the NOAA RTG SST, greatly improving forecasts in the vicinity of these lakes.

g. Smoke initialization for HRRRv4

Identification of fire locations within the HRRR domain is provided by hotspots detected by polar-orbiting satellites (Ahmadov et al. 2017). The HRRR uses data from the VIIRS instrument aboard the *Suomi NPP* and *NOAA-20* satellites, as well as by the Moderate Resolution Imaging Spectroradiometer (MODIS) instrument aboard NASA satellites *Aqua* and *Terra*. Currently, the HRRR uses fire hotspots collected over the previous 24 h. Once the satellite fire detection data are obtained, the hotspots are mapped onto the 3-km HRRR grid, along with an associated "fire radiative power" (FRP) determined by the detecting instrument. From this point, biomass burning emissions and smoke plume evolution are parameterized based upon the measured FRP as well as the underlying land surface type. Point sources of PM2.5 are then introduced into the HRRR forecast with diurnally varying emissions. Once the smoke tracer is included in the 3D HRRR grid, the HRRR provides a forecast of the evolution of the smoke plume based upon the atmospheric conditions.

4. High-impact weather prediction examples using HRRR

In this section, we provide examples illustrating the capabilities of the HRRR for predicting high-impact weather events from the past decade.

a. Aviation forecasting and CoSPA

The FAA Aviation Weather Research Program has led an effort over the last 20 years to simplify and consolidate the variety of forecast products available for aviation decision making. The advent of the HRRR enabled development of the CoSPA system (Wolfson et al 2008; section 1), a blend of heuristic-based extrapolation forecasts with HRRR forecasts.

CoSPA's focus on convective storms is attributable to the fact that weather-related delays account for nearly 70% of total delays in the U.S. National Airspace System, and convective weather accounts for 60% of these weather delays (Klingle-Wilson and Evans 2005). The problem is particularly acute in the northeastern portion of the NAS, due to enroute and terminal congestion and an associated lack of excess capacity available for delaying or rerouting aircraft. Benefits from more accurate forecasts of aviation-relevant parameters such as VIL and ET include more efficient use of air-traffic management initiatives and a reduced need for tactical action. Figure 4 provides an example of a successful VIL forecast from the HRRR, as compared against MRMS-analyzed VIL, for a potentially high-impact convective line passing through the northeastern NAS on 14 July 2016. The HRRR accurately forecasts the porosity of the significant convective line passing through New York and captures the position of a stronger cell in northwestern New Jersey as well. The 6–12 h of advance warning of this feature permitted air traffic managers to anticipate effects on arrivals and departures from New York City area terminals, minimizing air traffic delays due to several hours of aircraft rerouting. VIL forecasts from the HRRR were used directly in CoSPA for forecast lengths greater than 2 h.

b. Severe weather forecasting

On 10 August 2020, a derecho (Johns and Hirt 1987) struck the U.S. Midwest, producing $10+ billion in damage to homes, businesses, utility infrastructure, and crops (NOAA/NCEI 2022). The derecho was particularly severe at midday in eastern Iowa (Fig. 5e), producing estimated surface winds exceeding 60 m s^{-1} in the Cedar Rapids, Iowa, area (NWS 2020).

The Midwest derecho was not anticipated far in advance. Outlooks issued by the SPC at 1730 UTC 9 August and 0600 UTC 10 August indicated only a marginal risk of severe weather from Iowa into northern Illinois; at 1300 UTC 10 August, the risk was upgraded to enhanced (not shown). HRRR forecasts initialized before 0000 UTC 10 August provided no clear guidance, showing a variety of scenarios for the convective-storm evolution in the Midwest (not shown).

We focus here on forecasts initialized between 0300 and 0900 UTC 10 August (Figs. 1c, 5), with lead times of 6–24 h, a
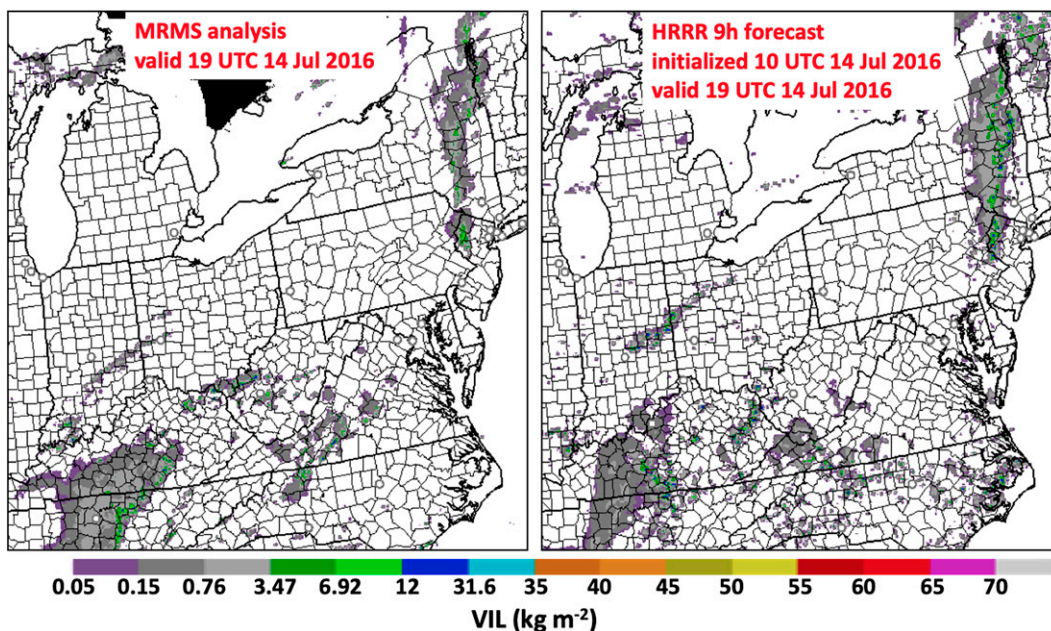
FIG. 4. (right) Real-time experimental HRRRv2 9-h forecast of vertically integrated liquid (kg m^{-2}) compared against (left) MRMS analysis, both valid at 1900 UTC 14 Jul 2016.

key situational-awareness and short-range-forecasting time frame for the NWS SPC and Weather Forecast Offices. By this time, HRRR forecasts were consistently indicating a daytime convective system that would affect Iowa and Illinois. The derecho occurred while both the operational HRRRv3 and experimental (soon to be operational) HRRRv4 were running, providing an opportunity to compare forecasts from the two systems. The comparisons in Fig. 5 focus on the reflectivity structure and the swaths of maximum surface winds associated with the convective system. The experimental HRRRv4 forecasts (Figs. 5c,d) indicated a more organized and more realistic reflectivity structure than the HRRRv3 (Figs. 5a,b) forecasts, in terms of a more extensive high-reflectivity leading line exhibiting bowing characteristics and a more extensive trailing stratiform region. Forecasts from both HRRR versions tended to be too slow to move the system through Iowa, though (e.g., Figs. 5b,d,e).

The derecho produced surface winds exceeding 35 m s^{-1} over a wide swath from central Iowa to northern Illinois (NWS 2020). Compared to HRRRv3, the experimental HRRRv4 forecasts provided more realistic guidance about where these severe winds would occur (orange and red colors in Iowa and Illinois in Figs. 5i–k). Although the HRRRv3 forecasts also indicated a threat of severe winds, these forecasts tended to emphasize Illinois more than Iowa (Figs. 5g,h) and indicated only small areas of strong winds in Iowa (Figs. 5f,g). Overall, it is encouraging to see that the experimental HRRRv4 provided more realistic forecasts for this case. Determining which specific changes to the HRRR system contributed most to the improved forecasts would require further investigation, beyond the scope of this article.

c. Quantitative precipitation forecasting

On 23 June 2016, an MCS impacted West Virginia. Convection continually redeveloped to the rear of the MCS for about 18 h, producing torrential rain over the complex terrain of central West Virginia. The resulting runoff produced catastrophic flooding, leading to 23 fatalities and extensive property damage (Martinaitis et al. 2020). During a 24-h period ending 0000 UTC 24 June, storm-total rainfall exceeded 3.0 in. over a northwest–southeast swath from central Ohio through central West Virginia into central Virginia and exceeded 6.0 in. over a small area in southern West Virginia (Fig. 6). An experimental HRRRv2 3–27-h forecast of the event captured the main features of the Stage-IV QPE well, including the spatial extent of the 3+ in. rainfall amounts, as well as small areas of 6+ in. totals in West Virginia, although these regions of heaviest rain are forecast slightly too far north.

d. Winter weather forecasting

Winter weather hazards represent a significant forecasting challenge in much of the United States. Hazards include subfreezing or extreme cold temperatures, limited vehicle traction due to ice or snow buildup on roads, low visibility due to fog or snow (whether falling or blowing), and high winds. The SPC provides winter weather mesoscale discussions, and local forecast offices within the NWS issue winter weather advisories and winter storm watches/warnings. Many winter weather impacts occur in conjunction with "nor'easter" snowstorms on the east coast of the United States (Kocin and Uccellini 2004). The HRRR system provides forecast guidance on all the hazards related to these systems in the day 1 to day 2 time frame.
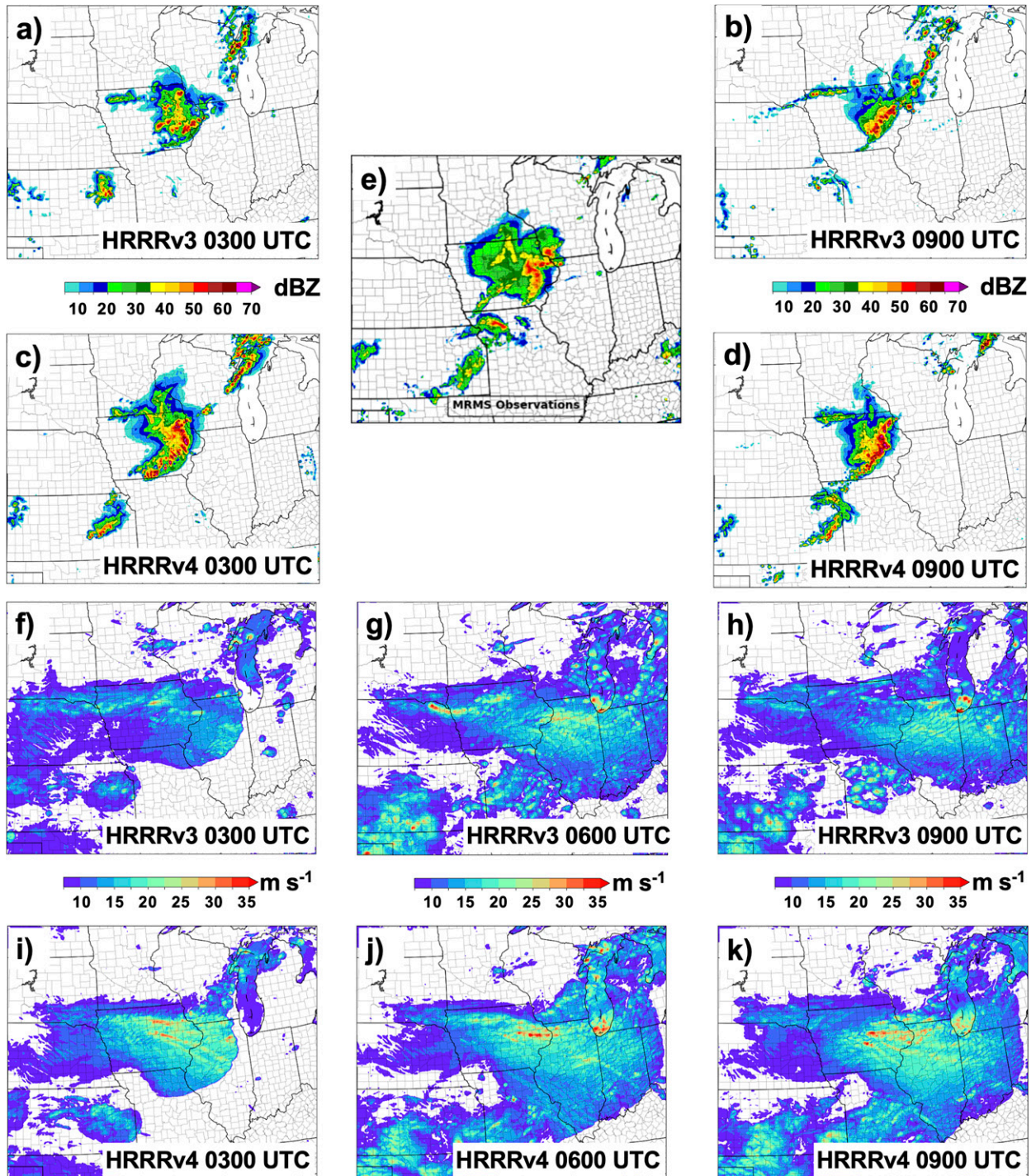
FIG. 5. (a),(b),(f),(g),(h) Operational HRRRv3 and (c),(d),(i),(j),(k) experimental HRRRv4 forecasts for the 10 Aug 2020 derecho. Composite radar reflectivity (dBZ) at 1800 UTC is shown for HRRR forecasts initialized at 0300 UTC in (a) and (c), HRRR forecasts initialized at 0900 UTC in (b) and (d), and MRMS observations in (e). Maximum 10-m wind speeds (m s^{-1}) during 0–18-h forecasts are shown for HRRR forecasts initialized at 0300 UTC in (f) and (i), 0600 UTC in (g) and (j), and 0900 UTC in (h) and (k).
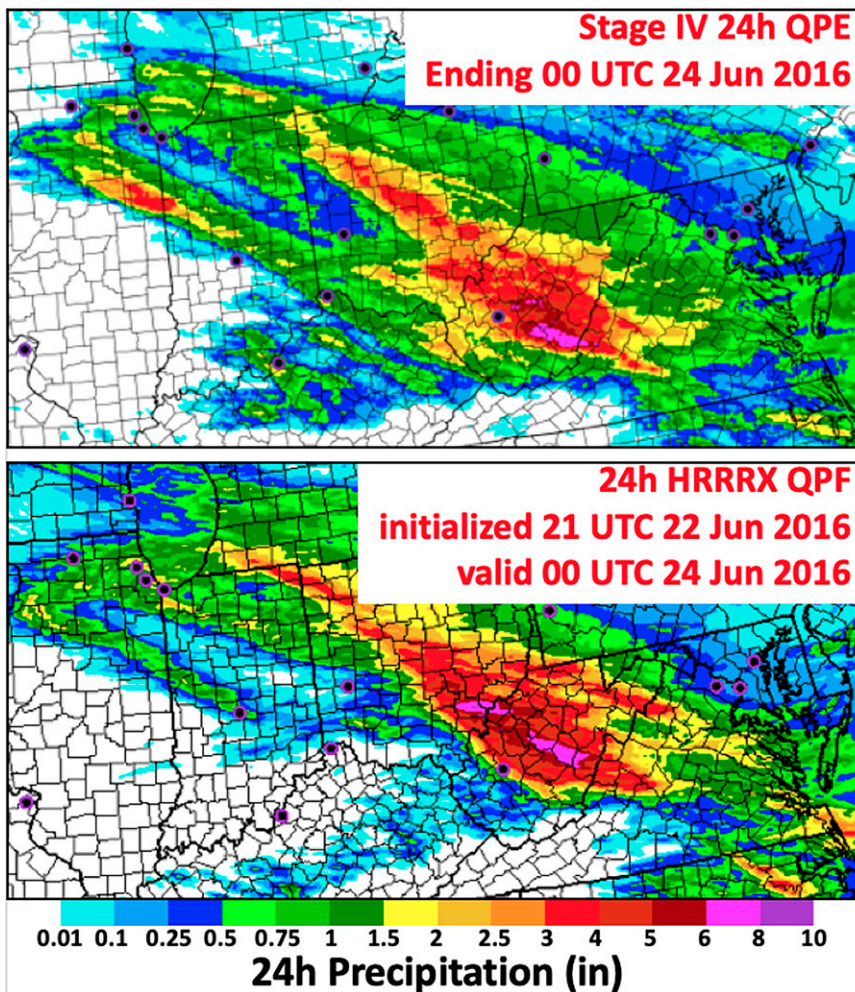
FIG. 6. (top) Stage-IV QPE (in.) and (bottom) experimental HRRRv2 QPF (in.) for the 24-h period ending at 0000 UTC 24 Jun 2016.

In late January 2016, a particularly strong extratropical cyclone developed over the eastern United States, following a track historically associated with other large snowstorms (Leathers et al. 1998). The storm set new snowfall records in several major East Coast cities, including Baltimore, Maryland; Harrisburg, Pennsylvania; Newark, New Jersey; and New York City, New York. States of emergency were declared in 11 states, and more than 13 000 flights were canceled in association with the storm.

Spatial verification of snowfall is difficult due to several factors, including melting, sublimation, compaction, and drifting of snow. The summed snowfall in three 24-h forecasts from the experimental HRRRv2 (22, 23, and 24 January 2016, each initialized at 0600 UTC) are compared with the NCEI 72-h snowfall analysis (Fig. 7). For one comparison, the HRRR snowfall is derived by applying the typical 10:1 conversion factor to the equivalent amount of liquid water reaching the ground as snow (middle panel of Fig. 7). The HRRR successfully captured the main axis of the storm, with totals of 20+ in. in a swath from West Virginia through the Washington, D.C., area into the New York City region.

An alternative comparison uses a variable snow density calculation for the snowfall accumulation during the HRRR forecasts (bottom panel in Fig. 7). The variable density calculation improves the snowfall forecast in the eastern portion of the snowfall swath, increasing the snowfall forecast in southeastern Pennsylvania while reducing amounts in southern New England. The variable density calculation also results in more snowfall forecast in northern Virginia, in better agreement with the snowfall analysis. However, the extent of the 30+ in. snowfall appears overdone by the HRRR forecast. The variable density algorithm shown here is the one present in HRRRv2-v3; the relationship between snow density and near-surface temperature was refined in HRRRv4 (Benjamin et al. 2021b), most notably producing greater accumulations when temperatures are near 0°C.

e. Landfalling tropical cyclone hazard forecasting

The Gulf and East Coasts of the United States are vulnerable to hazards from landfalling tropical cyclones (TCs), with massive human and economic impacts [e.g., Hurricane Katrina in 2005 (Beven et al. 2008); Hurricane Sandy in 2012
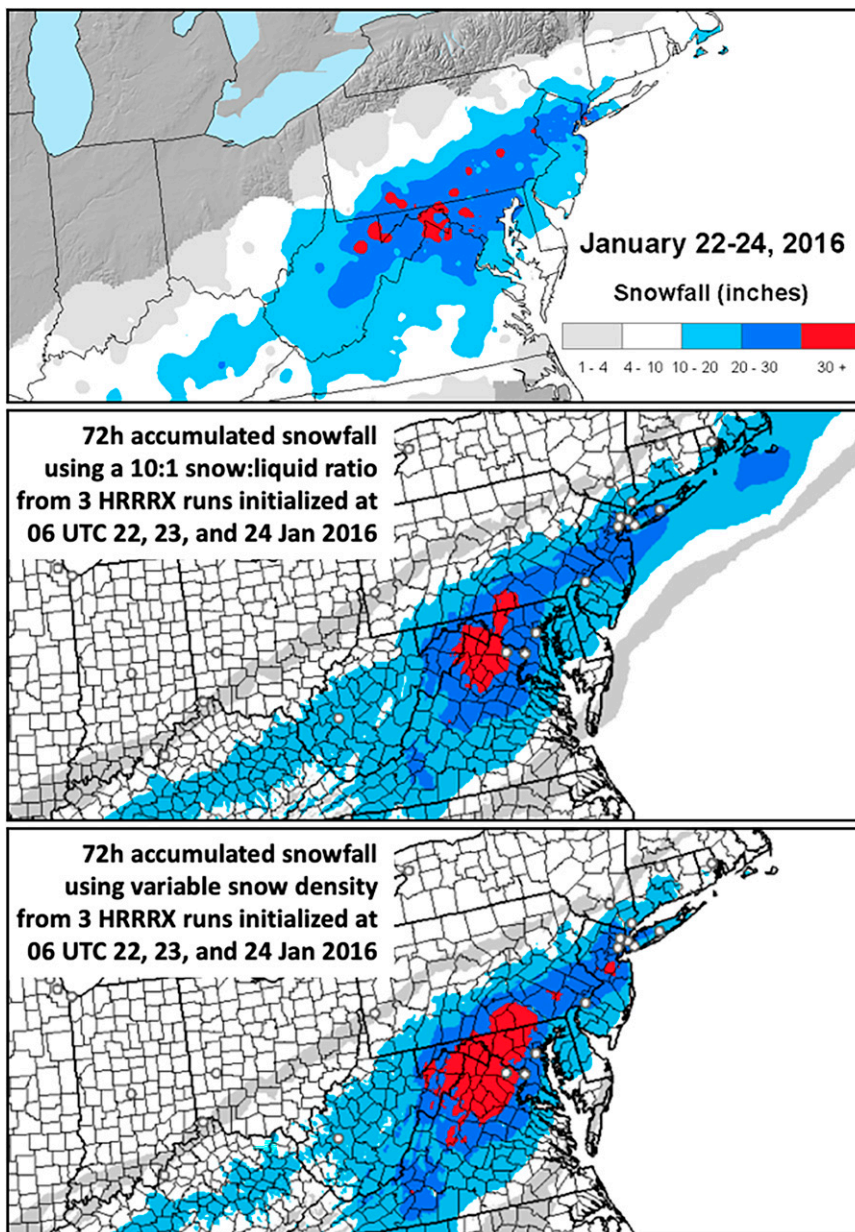
Fig. 7. (top) Observed snowfall analysis (in.) and (bottom) 72-h accumulated snowfall forecast by the experimental HRRRv2 using two different accumulation methods, for the 72-h period ending at 0600 UTC 24 Jan 2016.

(Uccellini 2013)]. The National Hurricane Center issues track and intensity forecasts for TCs in both the Atlantic and the eastern Pacific basins. The HRRR is well positioned to provide forecasts of TC hazards at landfall as storms approach the U.S. coast.

Hurricane Harvey was the largest weather-related catastrophe of 2017 in the United States (NOAA/NCEI 2022), producing extensive storm-surge flooding and wind damage, followed by prodigious inland rainfall totals over southeastern Texas. Devastating flooding impacted the Houston, Texas,

metropolitan area as Harvey moved slowly eastward across the area.

The 48-h experimental HRRRv3 initialized at 1200 UTC 24 August 2017 forecast the storm track accurately and successfully indicated rainfall totals exceeding 10 in. Some noteworthy details were incorrect, such as advancing the heavy rain too quickly toward Houston, and underestimating the rainfall totals near the hurricane center (Figs. 8a,b). A subsequent 48-h experimental HRRRv3 forecast, initialized at 1200 UTC 26 August 2017, captured the swath of 20+ in. 48-h
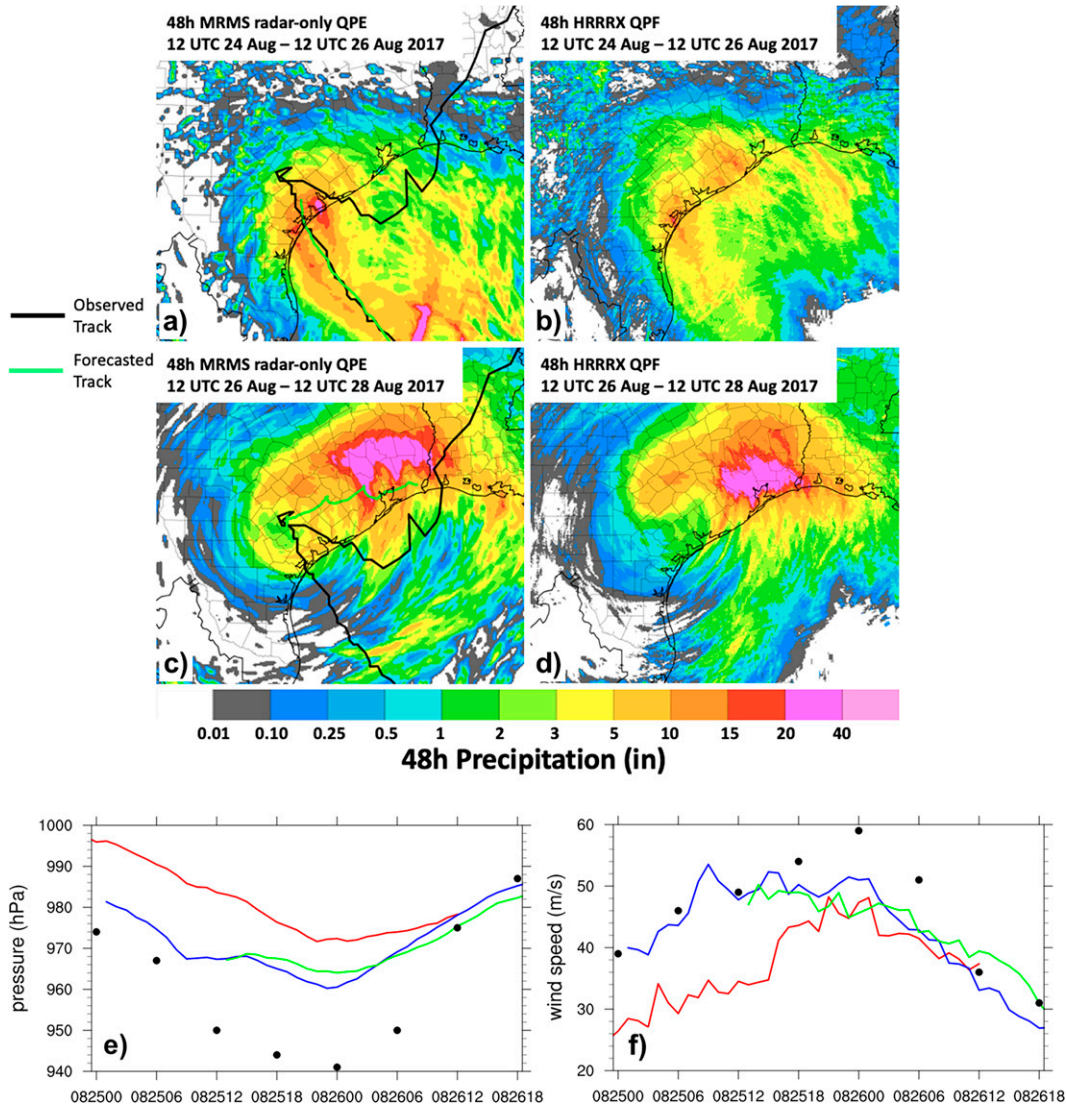
FIG. 8. Experimental HRRRv3 forecasts and verification for Hurricane Harvey in August 2017. The 48-h QPF (in.) from the forecasts initialized at (b) 1200 UTC 24 Aug and (d) 1200 UTC 26 Aug are compared to (a),(c) 48-h MRMS radar-only QPE during the same time periods. Observed (from National Hurricane Center; black) and forecast (HRRR; green) tracks of the central pressure minimum are also shown. (e),(f) The minimum central pressure (hPa) and hourly maximum 10-m wind speeds (m s^{-1}) are shown for the experimental HRRRv3 forecasts initialized at 1200 UTC 24 Aug (red), 0000 UTC 25 Aug (blue), and 1200 UTC 25 Aug (green). TCVitals estimates of these quantities every 6 h are shown with black dots.

rainfall over far southeastern Texas remarkably well (Figs. 8c,d). The east–west orientation of the heaviest rainfall, as well as the westward extension of the 5–10-in. rainfall amounts to the west of Houston, were forecast successfully. The HRRR forecast the heaviest rainfall slightly farther south than where it was observed but nonetheless indicated the potential for catastrophic amounts of rain over a multiday period.

Verification of HRRR forecasts of minimum pressure and maximum surface winds for Harvey (Figs. 8e,f) is consistent with our qualitative impressions of HRRR forecast performance for landfalling tropical cyclones in general during the last several years: typically helpful for identifying periods of strengthening and weakening, but with large errors in storm intensity. The HRRR forecasts of Harvey initialized at 1200 UTC 24 August and 0000 UTC 25 August (red and blue lines in Figs. 8e,f) indicate storm strengthening before landfall but overestimate minimum pressure and underestimate maximum wind by as much as 30 hPa and 15 m s^{-1}, respectively.

f. Dense smoke pollution

Owing to impacts of smoke on air quality and health, visibility and transportation, solar-energy production, and weather, accurate smoke forecasts are of significant value (James et al. 2019). As described in section 2d, HRRRv4
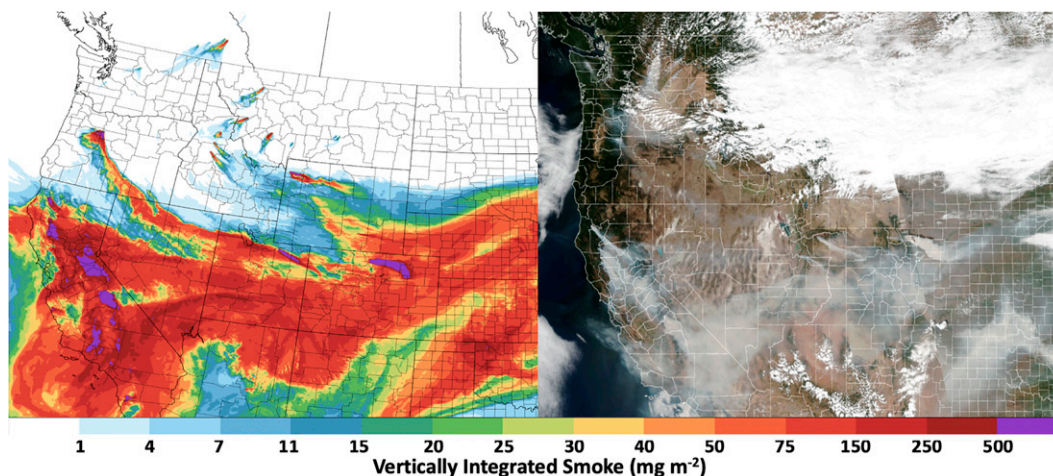
FIG. 9. (a) The 21-h experimental HRRRv4 forecast of vertically integrated smoke (mg m^{-2}) valid at 2100 UTC 7 Sep 2020, compared with (b) visible polar-orbiting satellite imagery from 7 Sep 2020.

includes prediction of smoke in terms of PM2.5. We compare an example experimental HRRRv4 forecast of vertically integrated smoke (Fig. 9a) to visible satellite imagery (Fig. 9b) during the significant 2020 fire season in the western CONUS. Fires in Colorado and Utah that had been burning since July and August 2020, as well as more recent lightning-ignited fires in Washington, Oregon, and California, displayed active behavior with large smoke plumes transporting smoke pollution far downstream. The experimental forecast captured both the national scale of the resulting smoke coverage, as well as the location and orientation of some of the major smoke plumes. For 9-h forecasts valid at 2100 UTC 7 September (cf. Fig. 9a), the experimental HRRRv4 (with smoke) produced surface temperatures as much as 10 K less than the operational HRRRv3 (without smoke) beneath the plume of the Cameron Peak Fire in northern Colorado (not shown).

g. Wind-energy forecasting

The high spatial resolution and rapid-update nature of the HRRR make it an ideal tool for the wind-energy community, which needs to consider and frequently reassess day-ahead forecasts to more efficiently integrate wind-produced energy into the electrical grid. Cases in which the forecast wind is higher than the actual wind are particularly troublesome because more wind energy is anticipated than can be delivered, forcing the energy provider to produce or purchase the "missing energy" from other sources. Thus, the energy community is very sensitive to rapid decreases (down ramp events, Bianco et al 2016) in the wind speed because of the significant economic impact of these events (Turner et al. 2022).

A case on 11 August 2019 shows the ability of the experimental HRRRv4 to accurately forecast a significant down ramp event in a region where there are many wind turbines (Fig 10). The down ramp at the observing site in northern Oklahoma (red square in top panel of Fig. 10) started just

after 1200 UTC (bottom panel of Fig. 10). While the forecast initialized at 0000 UTC 10 August did not capture the down ramp, the forecast initialized at 0600 UTC 10 August, as well as each subsequent forecast, captured this down-ramp event. The consistency of these forecasts allows the energy community to have confidence in forecast ramp events (and overall wind-energy predictions), and allows them the time to bring other energy sources (e.g., fossil-fuel generation) online to compensate for the lack of wind-produced power.

5. Conclusions

The HRRR system represents a culmination of nearly three decades of development on frequently updated NWP systems within NOAA. The RUC system (operational 1994–2012; Benjamin et al. 2004), initially developed to take advantage of frequent aircraft-based observations, paved the way for development of the community-based hourly RAP system and its use of satellite radiance observations from polar-orbiting satellites, providing forecasters with low-latency, hourly updated mesoscale model analyses and forecasts, as compared with 6-hourly updated modeling systems. With 3-km grid spacing, the HRRR system provided the opportunity to better represent convection and its associated hazards. The HRRR was first employed by aviation forecasters to aid with both strategic and tactical decision making, with more recent applications emerging such as severe weather forecasting, renewable-energy generation forecasting, and flash flood forecasting. A quantitative evaluation of the HRRR forecast performance is provided in the companion paper, part two of this two-part series (James et al. 2022).

Important to its application for short-range forecasting is the design of the HRRR initialization. The HRRR system has evolved significantly over the years, but use of radar-reflectivity observations as well as hybrid ensemble-variational data assimilation, originally with ensemble covariances from GDAS but more recently from the HRRRDAS convection-allowing ensemble, are key to initializing convective storms and their
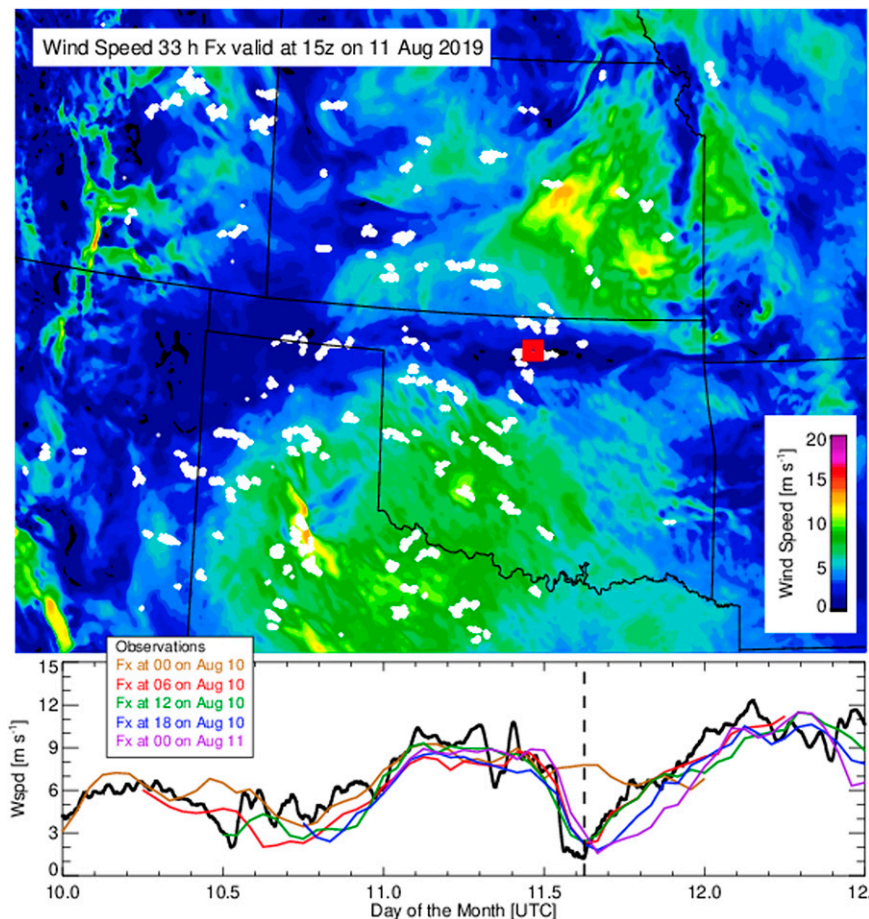
FIG. 10. (top) Wind speed at 80 m above ground level for a 33-h experimental HRRRv4 forecast valid at 1500 UTC 11 Aug 2019, and (bottom) the wind speeds at 60 m above ground forecast at the ARM Southern Great Plains site (red square) from multiple model initialization times compared to the observed wind speed on a 60-m tower at the ARM site (black line). The vertical dashed line denotes the valid time for the spatial map in the upper panel. The white symbols denote the locations of wind turbines.

environments. A non-variational cloud analysis has been very effective in initializing stratiform clouds to improve the surface energy balance driving PBL evolution, and provides a baseline for evaluation of more advanced cloud initialization procedures in the future. Overall, data assimilation for multiple components of the Earth system (mesoscale and synoptic-scale atmosphere, clouds and convective storms, land, lakes, smoke) are essential for the effective application to short-range prediction problems.

The use of community-supported software within the HRRR data assimilation and dynamical model core has provided an important link between the operational and research communities during the development of the HRRR. For example, the use of GSI for the HRRR has enabled the use of hybrid ensemble-variational data assimilation at the 3-km scale, with significant associated forecast improvements. Similarly, the use of the community WRF-ARW non-hydrostatic model opened the door for effective 3-km storm prediction.

Finally, community physics parameterizations within WRF-ARW were essential for HRRR such as the development at NCAR on the Thompson microphysics scheme and at Atmospheric and Environmental Research on the radiation parameterization RRTMG. Similarly, mutual benefit to the NOAA HRRR/RAP models and the larger WRF community resulted from development of the RUC land surface model and scale awareness within the MYNN PBL and surface layer schemes.

HRRR output is distributed to users via many different avenues, with forecast grids available in real time from NCEP in GRIB2 format. Until recently, the only publicly available data archive was hosted by the University of Utah, featuring novel data access solutions for interrogating a large data volume (Blaylock et al. 2017). This archive has recently been transitioned to Amazon Web Services, while Google has also developed an archive on their Cloud Platform.

Many aspects of the future RRFS will be based on data-assimilation and forecasting methods developed for the

HRRR, and the operational HRRRv4, along with other present-day operational CAMs, will provide a baseline for forecast performance for evaluating the RRFS as it is being developed. The 3-km RRFS domain will cover a much larger area than the HRRR, including the CONUS and Alaska. When the RRFS becomes operational, both the HRRRv4 CONUS and Alaska systems will be discontinued. The large RRFS domain will allow improved treatment of approaching tropical cyclones from the Caribbean, the simulation of high-resolution smoke transport through the complex terrain of western Canada, and the prediction of rainfall and snowfall in the northern reaches of the Columbia River watershed, which influences streamflow for hydroelectric production in Washington and Oregon. The larger domain will also require additional physics and data assimilation development for representing weather in the tropics, maritime regions, and the Arctic; such development is critical for the future deployment of a global rapid refresh NWP capability. For local regions and specific types of weather, higher-resolution forecasting will be required. The related WoF project will particularly evaluate sub-kilometer grid spacing for convective-storm forecasting (Bryan et al. 2003), with a target of 250 m proposed by Stensrud et al. (2009).

The planned RRFS will be an ensemble system, enabling advanced DA and providing forecasts with explicit uncertainty information and increased ability to detect rare, high-impact weather events. Valuable experience with storm-scale ensembles has been gained during the HRRR era (e.g., Kalina et al. 2021), but numerous challenges lie ahead with developing sharp and reliable ensemble-forecast capabilities in a single-model system.

APPENDIX

Acronyms and Abbreviations

BEC	Background-error covariances
CAM	Convection-allowing model
CFL	Courant–Friedrichs–Lewy
CIWS	Corridor Integrated Weather System
CLM	Community Land Model
CONUS	Conterminous United States
CoSPA	Consolidated Storm Prediction for Aviation
DA	Data assimilation
DFI	Digital filter initialization
EDMF	Eddy-diffusivity/mass-flux
EnKF	Ensemble Kalman filter
EnSRF	Ensemble square-root filter
EnVar	Ensemble–variational
ET	Echo tops
FAA	Federal Aviation Administration
FRP	Fire radiative power
FVCOM	Finite Volume Community Ocean Model
GDAS	Global Data Assimilation System
GFS	Global Forecast System
GPS	Global positioning system
GSI	Gridpoint Statistical Interpolation
GSL	Global Systems Laboratory
GVF	Greenness vegetation fraction
HRRR	High-Resolution Rapid Refresh
HRRRDAS	HRRR Data-Assimilation System
IEVA	Implicit-explicit vertical advection
LAMP	Localized Aviation Model Output Statistics Program
LSM	Land surface model
MCS	Mesoscale convective system
MODIS	Moderate Resolution Imaging Spectroradiometer
MRMS	Multi-Radar Multi-Sensor
MYNN	Mellor–Yamada–Nakanishi–Niino
NBM	National Blend of Models
NCEP	National Centers for Environmental Prediction
NOAA	National Oceanic and Atmospheric Administration
NWP	Numerical weather prediction
NWS	National Weather Service
PBL	Planetary boundary layer
PM2.5	Particulate matter less than 2.5 μm
QPE	Quantitative precipitation estimation

QPF	Quantitative precipitation forecast
RAP	Rapid Refresh
RRFS	Rapid Refresh Forecast System
RRTMG	Rapid Radiative Transfer Model for general circulation models
RTG	Real-Time Global
RTMA	Real-Time Mesoscale Analysis
RUC	Rapid Update Cycle
SCHDA	Stratiform cloud-hydrometeor data assimilation
SGS	Subgrid scale
SPC	Storm Prediction Center
SST	Sea surface temperature
TC	Tropical cyclone
UFS	Unified Forecast System
VIIRS	Visible Infrared Imaging Radiometer Suite
VIL	Vertically integrated liquid
WCOSS	Weather and Climate Operational Supercomputing System
WoF	Warn-on-Forecast
WPS	WRF Preprocessing System
WRF-ARW	Advanced Research version of the Weather Research and Forecasting Model

REFERENCES

Ahmadov, R., and Coauthors, 2017: Using VIIRS fire radiative power data to simulate biomass burning emissions, plume rise and smoke transport in a real-time air quality modeling system. *Proc. 2017 IEEE Int. Geoscience and Remote Sensing Symp. (IGARSS)*, Fort Worth, TX, IEEE, 2806–2808, https://doi.org/10.1109/IGARSS.2017.8127581.

Anderson, E. J., A. Fujisaki-Manome, J. Kessler, G. A. Lang, P. Y. Chu, J. G. W. Kelley, Y. Chen, and J. Wang, 2018: Ice forecasting in the next-generation Great Lakes Operational Forecast System (GLOFS). *J. Mar. Sci. Eng.*, **6**, 123, https://doi.org/10.3390/jmse6040123.

Arthur, R. S., K. A. Lundquist, and J. B. Olson, 2021: Improved prediction of cold air pools in the Weather Research and Forecasting Model using a truly horizontal diffusion scheme for potential temperature. *Mon. Wea. Rev.*, **149**, 155–171, https://doi.org/10.1175/MWR-D-20-0234.1.

Arulaj, M., and A. P. Barros, 2021: Automatic detection and classification of low-level orographic precipitation processes from space-borne radars using machine learning. *Remote Sens. Environ.*, **257**, 112355, https://doi.org/10.1016/j.rse.2021.112355.

Baldauf, M., A. Siefert, J. Forstner, D. Majewski, M. Raschendorfer, and T. Reinhardt, 2011: Operational convective-scale numerical weather prediction with the COSMO model: Description and sensitivities. *Mon. Wea. Rev.*, **139**, 3887–3905, https://doi.org/10.1175/MWR-D-10-05013.1.

Beck, J., and Coauthors, 2020: An evaluation of a hybrid, terrain-following vertical coordinate in the WRF-based RAP and HRRR models. *Wea. Forecasting*, **35**, 1081–1096, https://doi.org/10.1175/WAF-D-19-0146.1.

Beljaars, A. C. M., A. R. Brown, and N. Wood, 2004: A new parameterization of turbulent orographic form drag. *Quart. J. Roy. Meteor. Soc.*, **130**, 1327–1347, https://doi.org/10.1256/qj.03.73.

Benjamin, S. G., and Coauthors, 2004: An hourly assimilation-forecast cycle: The RUC. *Mon. Wea. Rev.*, **132**, 495–518, https://doi.org/10.1175/1520-0493(2004)132<0495:AHACTR>2.0.CO;2.

——, and Coauthors, 2016: A North American hourly assimilation and model forecast cycle: The Rapid Refresh. *Mon. Wea. Rev.*, **144**, 1669–1694, https://doi.org/10.1175/MWR-D-15-0242.1.

——, J. M. Brown, G. Brunet, P. Lynch, K. Saito, and T. W. Schlatter, 2019: 100 years of progress in forecasting and NWP applications. *A Century of Progress in Atmospheric and Related Sciences: Celebrating the American Meteorological Society Centennial, Meteor. Monogr.*, No. 59, Amer. Meteor. Soc., https://journals.ametsoc.org/doi/pdf/10.1175/AMSMONOGRAPHS-D-18-0020.1.

——, and Coauthors, 2021a: Stratiform cloud-hydrometeor assimilation for HRRR and RAP model short-range weather prediction. *Mon. Wea. Rev.*, **149**, 2673–2694, https://doi.org/10.1175/MWR-D-20-0319.1.

——, E. P. James, J. M. Brown, E. J. Szoke, J. S. Kenyon, R. Ahmadov, and D. D. Turner, 2021b: Diagnostic fields developed for hourly updated NOAA weather models. NOAA Tech. Memo OAR GSL-66, 55 pp., https://doi.org/10.25923/f7b4-rx42.

——, T. G. Smirnova, E. P. James, E. J. Anderson, A. Fujisaki-Manomi, J. G. W. Kelley, G. E. Mann, A. D. Gronewold, P. Chu, and S. G. T. Kelley, 2022a: Inland lake temperature initialization via coupled cycling with atmospheric data assimilation. *Geosci. Model Dev.*, **15**, 6659–6676, https://doi.org/10.5194/gmd-15-6659-2022.

——, ——, ——, L.-F. Lin, M. Hu, D. D. Turner, and S. He, 2022b: Land-snow assimilation including a moderately coupled initialization method applied to NWP. *J. Hydrometeor.*, **23**, 825–845, https://doi.org/10.1175/JHM-D-21-0198.1.

Bernardet, L., and Coauthors, 2008: The Developmental Testbed Center and its Winter Forecasting Experiment. *Bull. Amer. Meteor. Soc.*, **89**, 611–628, https://doi.org/10.1175/BAMS-89-5-611.

Beven, J. L., II, and Coauthors, 2008: Atlantic hurricane season of 2005. *Mon. Wea. Rev.*, **136**, 1109–1173, https://doi.org/10.1175/2007MWR2074.1.

Bianco, L., and Coauthors, 2016: A wind energy ramp tool and metric for measuring the skill of numerical weather prediction models. *Wea. Forecasting*, **31**, 1137–1156, https://doi.org/10.1175/WAF-D-15-0144.1.

Blaylock, B. K., J. D. Horel, and S. T. Liston, 2017: Cloud archiving and data mining of high-resolution Rapid Refresh forecast model output. *Comput. Geosci.*, **109**, 43–50, https://doi.org/10.1016/j.cageo.2017.08.005.

Brousseau, P., Y. Seity, D. Ricard, and J. Leger, 2016: Improvement of the forecast of convective activity from the AROME-France system. *Quart. J. Roy. Meteor. Soc.*, **142**, 2231–2243, https://doi.org/10.1002/qj.2822.

Brown, A., S. Milton, M. Cullen, B. Golding, J. Mitchell, and A. Shelly, 2012: Unified modeling and prediction of weather and climate: A 25-year journey. *Bull. Amer. Meteor. Soc.*, **93**, 1865–1877, https://doi.org/10.1175/BAMS-D-12-00018.1.

Bryan, G. H., J. C. Wyngaard, and J. M. Fritsch, 2003: Resolution requirements for the simulation of deep moist convection. *Mon. Wea. Rev.*, **131**, 2394–2416, https://doi.org/10.1175/1520-0493(2003)131<2394:RRFTSO>2.0.CO;2.

Chaboureau, J.-P., and P. Bechtold, 2002: A simple cloud parameterization derived from cloud resolving model data: Diagnostic and prognostic applications. *J. Atmos. Sci.*, **59**,

2362–2372, https://doi.org/10.1175/1520-0469(2002)059<2362: ASCPDF>2.0.CO;2.

——, and ——, 2005: Statistical representation of clouds in a regional model and the impact on the diurnal cycle of convection during Tropical Convection, Cirrus and Nitrogen Oxides (TROCCINOX). *J. Geophys. Res.*, **110**, D17103, https://doi. org/10.1029/2004JD005645.

Chen, C., R. C. Beardsley, and G. Cowles, 2006: An unstructured grid, finite volume coastal ocean model (FVCOM) system. *Oceanography*, **19**, 78–89, https://doi.org/10.5670/oceanog. 2006.92.

Clark, A. J., and Coauthors, 2012: An overview of the 2010 Hazardous Weather Testbed Experimental Forecast Program Spring Experiment. *Bull. Amer. Meteor. Soc.*, **93**, 55–74, https://doi.org/10.1175/BAMS-D-11-00040.1.

De Pondeca, M. S. F. V., and Coauthors, 2011: The real-time mesoscale analysis at NOAA's National Centers for Environmental Prediction: Current status and development. *Wea. Forecasting*, **26**, 593–612, https://doi.org/10.1175/WAF-D-10-05037.1.

Done, J., C. A. Davis, and M. L. Weisman, 2004: The next generation of NWP: Explicit forecasts of convection using the Weather Research and Forecasting (WRF) model. *Atmos. Sci. Lett.*, **5**, 110–117, https://doi.org/10.1002/asl.72.

Dowell, D. C., and Coauthors, 2016: Development of a High-Resolution Rapid Refresh Ensemble (HRRRE) for severe weather forecasting., *28th Conf. on Severe Local Storms,* Portland, OR, Amer. Meteor. Soc., 8B.2, https:// ams.confex.com/ams/28SLS/webprogram/Paper301555.html.

English, J. M., D. D. Turner, T. I. Alcott, W. R. Moninger, J. L. Bytheway, R. Cifelli, and M. Marquis, 2021: Evaluating operational and experimental HRRR model forecasts of atmospheric river events in California. *Wea. Forecasting*, **36**, 1925–1944, https://doi.org/10.1175/WAF-D-21-0081.1.

Erickson, M. J., J. S. Kastman, B. Albright, S. Perfater, J. A. Nelson, R. S. Schumacher, and G. R. Herman, 2019: Verification results from the 2017 HMT-WPC Flash Flood and Intense Rainfall Experiment. *J. Appl. Meteor. Climatol.*, **58**, 2591–2604, https://doi.org/10.1175/JAMC-D-19-0097.1.

Fujisaki-Manome, A., and Coauthors, 2020: Improvements to lake-effect snow forecasts using a one-way air-lake model coupling approach. *J. Hydrometeor.*, **21**, 2813–2828, https:// doi.org/10.1175/JHM-D-20-0079.1.

Glahn, B., A. D. Schnapp, J. E. Ghirardelli, and J.-S. Im, 2017: A LAMP-HRRR MELD for improved aviation guidance. *Wea. Forecasting*, **32**, 391–405, https://doi.org/10.1175/WAF-D-16-0127.1.

Grell, G. A., R. Knoche, R. Schmitz, S. A. McKeen, G. Frost, W. C. Skamarock, and B. Eder, 2005: Fully-coupled "online" chemistry within the WRF model. *Atmos. Environ.*, **39**, 6957–6976, https://doi.org/10.1016/j.atmosenv.2005.04.027.

Gross, M., and Coauthors, 2018: Physics–dynamics coupling in weather, climate, and earth system models: Challenges and recent progress. *Mon. Wea. Rev.*, **146**, 3505–3544, https://doi. org/10.1175/MWR-D-17-0345.1.

Gustafsson, N., and Coauthors, 2018: Survey of data assimilation methods for convective-scale numerical weather prediction at operational centres. *Quart. J. Roy. Meteor. Soc.*, **144**, 1218–1256, https://doi.org/10.1002/qj.3179.

Hagelin, S., J. Son, R. Swinbank, A. McCabe, N. Roberts, and W. Tennant, 2017: The Met Office convective-scale ensemble, MOGREPS-UK. *Quart. J. Roy. Meteor. Soc.*, **143**, 2846–1861, https://doi.org/10.1002/qj.3135.

Hamill, T. M., E. Engle, D. Myrick, M. Peroutka, C. Finan, and M. Scheuerer, 2017: The U.S. National Blend of Models for statistical postprocessing of probability of precipitation and deterministic precipitation amount. *Mon. Wea. Rev.*, **145**, 3441–3463, https://doi.org/10.1175/MWR-D-16-0331.1.

Hartman, B., H. Cutler, M. Shields, and D. Turner, 2021: The economic effects of improved precipitation forecasts in the United States due to better commuting decisions. *Growth Change*, **52**, 2149–2171, https://doi.org/10.1111/grow.12542.

Helfrich, S. R., D. McNamara, B. H. Ramsay, T. Baldwin, and T. Kasheta, 2007: Enhancements to, and forthcoming developments in the Interactive Multisensor Snow and Ice Mapping System (IMS). *Hydrol. Processes*, **21**, 1576–1586, https://doi. org/10.1002/hyp.6720.

Houtekamer, P. L., and F. Zhang, 2016: Review of the ensemble Kalman filter for atmospheric data assimilation. *Mon. Wea. Rev.*, **144**, 4489–4532, https://doi.org/10.1175/MWR-D-15-0440.1.

Hu, M., S. G. Benjamin, T. T. Ladwig, D. C. Dowell, S. S. Weygandt, C. R. Alexander, and J. S. Whitaker, 2017: GSI three-dimensional ensemble-variational hybrid data assimilation using a global ensemble for the regional Rapid Refresh model. *Mon. Wea. Rev.*, **145**, 4205–4225, https://doi.org/10.1175/MWR-D-16-0418.1.

Iacono, M., J. S. Delamere, E. J. Mlawer, M. W. Shepherd, S. A. Clough, and W. D. Collins, 2008: Radiative forcing by long lived greenhouse gases: Calculation with the AER radiative transfer models. *J. Geophys. Res.*, **113**, D13103, https://doi. org/10.1029/2008JD009944.

James, E. P., and S. G. Benjamin, 2017: Observation system experiments with the hourly updating Rapid Refresh model using GSI hybrid ensemble-variational data assimilation. *Mon. Wea. Rev.*, **145**, 2897–2918, https://doi.org/10.1175/MWR-D-16-0398.1.

——, ——, and M. Marquis, 2017: A unified high-resolution wind and solar dataset from a rapidly updating numerical weather prediction model. *Renewable Energy*, **102**, 390–405, https:// doi.org/10.1016/j.renene.2016.10.059.

——, and Coauthors, 2019: Rapidly-updating high-resolution predictions of smoke, visibility, and smoke-weather interactions using satellite fire products within the Rapid Refresh and High-Resolution Rapid Refresh coupled with smoke (RAP/ HRRR-smoke). *35th Conf. on Environmental Information Processing Technologies*, Phoenix, AZ, Amer. Meteor. Soc., 4B.3, https://ams.confex.com/ams/2019Annual/meetingapp.cgi/ Paper/353068.

——, and Coauthors, 2022: The High-Resolution Rapid Refresh (HRRR): An hourly updating convection-allowing forecast model. Part II: Forecast performance. *Wea. Forecasting*, in press, https://doi.org/10.1175/WAF-D-21-0130.1.

Johns, R. H., and W. D. Hirt, 1987: Derechos: Widespread convectively induced windstorms. *Wea. Forecasting*, **2**, 32–49, https://doi.org/10.1175/1520-0434(1987)002<0032:DWCIW>2. 0.CO;2.

Kain, J. S., and Coauthors, 2008: Some practical considerations regarding horizontal resolution in the first generation of operational convection-allowing NWP. *Wea. Forecasting*, **23**, 931–952, https://doi.org/10.1175/WAF2007106.1.

——, S. J. Weiss, J. J. Levit, M. E. Baldwin, and D. R. Bright, 2006: Examination of convection-allowing configurations of the WRF Model for the prediction of severe convective weather: The SPC/NSSL Spring Program 2004. *Wea. Forecasting*, **21**, 167–181, https://doi.org/10.1175/WAF906.1.

Kalina, E. A., I. Jankov, T. Alcott, J. Olson, J. Beck, J. Berner, D. Dowell, and C. Alexander, 2021: A progress report on the development of the high-resolution Rapid Refresh ensemble. *Wea. Forecasting*, **36**, 791–804, https://doi.org/10.1175/WAF-D-20-0098.1.

Kelleher, K. E., and Coauthors, 2007: Project CRAFT: A real-time delivery system for NEXRAD level-II data via the Internet. *Bull. Amer. Meteor. Soc.*, **88**, 1045–1057, https://doi.org/10.1175/BAMS-88-7-1045.

Kim, J.-H., R. D. Sharman, S. G. Benjamin, J. M. Brown, S.-H. Park, and J. Klemp, 2019: Improvement of mountain-wave turbulence forecasts in the NOAA's Rapid Refresh (RAP) model with hybrid vertical coordinate system. *Wea. Forecasting*, **34**, 773–780, https://doi.org/10.1175/WAF-D-18-0187.1.

Kleist, D. T., and K. Ide, 2015: An OSSE-based evaluation of hybrid variational–ensemble data assimilation for the NCEP GFS. Part I: System description and 3D-hybrid results. *Mon. Wea. Rev.*, **143**, 433–451, https://doi.org/10.1175/MWR-D-13-00351.1.

——, D. F. Parrish, J. C. Derber, R. Treadon, W.-S. Wu, and S. Lord, 2009: Introduction of the GSI into the NCEP Global Data Assimilation System. *Wea. Forecasting*, **24**, 1691–1705, https://doi.org/10.1175/2009WAF2222201.1.

Klemp, J. B., 2011: A terrain-following coordinate with smoothed coordinate surfaces. *Mon. Wea. Rev.*, **139**, 2163–2169, https://doi.org/10.1175/MWR-D-10-05046.1.

Klingle-Wilson, D., and J. E. Evans, 2005: Description of the Corridor Integrated Weather System (CIWS) weather products. Project Rep. ATC-317, MIT Lincoln Laboratory, Lexington, MA, 120 pp., https://www.ll.mit.edu/sites/default/files/publication/doc/2018-12/Klingle-Wilson_2005_ATC-317_WW-15318.pdf.

Knievel, J. C., G. H. Bryan, and J. C. Hacker, 2007: Explicit numerical diffusion in the WRF Model. *Mon. Wea. Rev.*, **135**, 3808–3824, https://doi.org/10.1175/2007MWR2100.1.

Kocin, P., and L. Uccellini, 2004: *Northeast Snowstorms. Vol. I: Overview*. Meteor. Monogr., No. 32, Amer. Meteor. Soc., 289 pp., https://doi.org/10.1175/0065-9401-32.54.1.

Lahmers, T. M., H. Gupta, C. L. Castro, D. J. Gochis, D. Yates, A. Dugger, D. Goodrich, and P. Hazenburg, 2019: Enhancing the structure of the WRF-Hydro hydrologic model for semi-arid environments. *J. Hydrometeor.*, **20**, 691–714, https://doi.org/10.1175/JHM-D-18-0064.1.

Leathers, D. J., D. R. Kluck, and S. Kroczynski, 1998: The severe flooding event of January 1996 across north-central Pennsylvania. *Bull. Amer. Meteor. Soc.*, **79**, 785–798, https://doi.org/10.1175/1520-0477(1998)079<0785:TSFEOJ>2.0.CO;2.

Lin, H., S. S. Weygandt, S. G. Benjamin, and M. Hu, 2017: Satellite radiance data assimilation within the hourly updated Rapid Refresh. *Wea. Forecasting*, **32**, 1273–1287, https://doi.org/10.1175/WAF-D-16-0215.1.

Marquis, M., J. Wilczak, M. Ahlstrom, J. Sharp, A. Stern, J. C. Smith, and S. Calvert, 2011: Forecasting the wind to reach significant penetration levels of wind energy. *Bull. Amer. Meteor. Soc.*, **92**, 1159–1171, https://doi.org/10.1175/2011BAMS3033.1.

Martinaitis, S. M., and Coauthors, 2020: The 23 June 2016 West Virginia flash flood event as observed through two hydrometeorology testbed experiments. *Wea. Forecasting*, **35**, 2099–2126, https://doi.org/10.1175/WAF-D-20-0016.1.

Milbrandt, J. A., S. Belair, M. Faucher, M. Vallee, M. L. Carrera, and A. Glazer, 2016: The pan-Canadian high-resolution (2.5 km) deterministic prediction system. *Wea. Forecasting*, **31**, 1791–1816, https://doi.org/10.1175/WAF-D-16-0035.1.

Miles, N. L., J. Verlinde, and E. E. Clothiaux, 2000: Cloud droplet size distributions in low-level stratiform clouds. *J. Atmos. Sci.*, **57**, 295–311, https://doi.org/10.1175/1520-0469(2000)057<0295:CDSDIL>2.0.CO;2.

Mishra, S., D. L. Mitchell, D. D. Turner, and R. P. Lawson, 2014: Parameterization of ice fall speeds in midlatitude cirrus: Results from SPartICus. *J. Geophys. Res. Atmos.*, **119**, 3857–3876, https://doi.org/10.1002/2013JD020602.

Nakanishi, M., and H. Niino, 2009: Development of an improved turbulence closure model for the atmospheric boundary layer. *J. Meteor. Soc. Japan.*, **87**, 895–912, https://doi.org/10.2151/jmsj.87.895.

Neggers, R. A. J., 2015: Exploring bin-macrophysics models for moist convective transport and clouds. *J. Adv. Model. Earth Syst.*, **7**, 2079–2104, https://doi.org/10.1002/2015MS000502.

NWS, 2020: August 10, 2020 derecho. NOAA/NWS, accessed 6 January 2022, https://www.weather.gov/dmx/2020derecho.

NOAA/NCEI, 2022: U. S. billion dollar weather and climate disasters. NOAA/NCEI, accessed 19 January 2022, https://doi.org/10.25921/stkw-7w73.

Olson, J. B., and Coauthors, 2019a: Improving wind energy forecasting through numerical weather prediction model development. *Bull. Amer. Meteor. Soc.*, **100**, 2201–2220, https://doi.org/10.1175/BAMS-D-18-0040.1.

——, J. S. Kenyon, W. M. Angevine, J. M. Brown, M. Pagowski, and K. Suselj, 2019b: A description of the MYNN-EDMF scheme and the coupling to other components in WRF-ARW. NOAA Tech. Memo. OAR GSD-61, 37 pp., https://repository.library.noaa.gov/view/noaa/19837.

——, T. Smirnova, J. S. Kenyon, D. D. Turner, J. M. Brown, W. Zheng, and B. Green, 2021: A description of the MYNN surface-layer scheme. NOAA Tech. Memo. OAR GSL-67, https://doi.org/10.25923/f6a8-bc75.

Oleson, K. W., and Coauthors, 2010: Technical description of version 4.0 of the Community Land Model (CLM). NCAR Tech. Note NCAR/TN-478+STR, 257 pp., https://doi.org/10.5065/D6FB50WZ.

Powers, J. G., and Coauthors, 2017: The Weather Research and Forecasting Model: Overview, system efforts, and future directions. *Bull. Amer. Meteor. Soc.*, **98**, 1717–1737, https://doi.org/10.1175/BAMS-D-15-00308.1.

Rasmussen, R., and Coauthors, 2011: High-resolution coupled climate runoff simulations of seasonal snowfall over Colorado: A process study of current and warmer climate. *J. Climate*, **24**, 3015–3048, https://doi.org/10.1175/2010JCLI3985.1.

Romine, G. S., C. S. Schwartz, J. Berner, K. R. Fossell, C. Snyder, J. L. Anderson, and M. L. Weisman, 2014: Representing forecast error in a convection-permitting ensemble system. *Mon. Wea. Rev.*, **142**, 4519–4541, https://doi.org/10.1175/MWR-D-14-00100.1.

Saito, K., and Coauthors, 2006: The operational JMA nonhydrostatic mesoscale model. *Mon. Wea. Rev.*, **134**, 1266–1298, https://doi.org/10.1175/MWR3120.1.

Schraff, C., H. Reich, A. Rhodin, A. Schomburg, K. Stephan, A. Perianez, and R. Potthast, 2016: Kilometre-scale ensemble data assimilation for the COSMO model (KENDA). *Quart. J. Roy. Meteor. Soc.*, **142**, 1453–1472, https://doi.org/10.1002/qj.2748.

Schwartz, C. S., and Z. Liu, 2014: Convection-permitting forecasts initialized with continuously cycling limited-area 3DVAR, ensemble Kalman filter, and "hybrid" variational-ensemble data

assimilation systems. *Mon. Wea. Rev.*, **142**, 716–738, https://doi.org/10.1175/MWR-D-13-00100.1.

——, and R. A. Sobash, 2019: Revisiting sensitivity to horizontal grid spacing in convection-allowing models over the central and eastern United States. *Mon. Wea. Rev.*, **147**, 4411–4435, https://doi.org/10.1175/MWR-D-19-0115.1.

——, G. S. Romine, and D. C. Dowell, 2021: Toward unifying short-term and next- day convection-allowing ensemble forecast systems with a continuously-cycling 3-km ensemble Kalman filter over the entire conterminous United States. *Wea. Forecasting*, **36**, 379–405, https://doi.org/10.1175/WAF-D-20-0110.1.

Seity, Y., P. Brousseau, S. Malardel, G. Hello, P. Benard, F. Bouttier, C. Lac, and V. Masson, 2011: The AROME-France convective-scale operational model. *Mon. Wea. Rev.*, **139**, 976–991, https://doi.org/10.1175/2010MWR3425.1.

Simonin, D., C. Pierce, N. Roberts, S. P. Ballard, and Z. Li, 2017: Performance of Met Office hourly cycling NWP-based nowcasting for precipitation forecasts. *Quart. J. Roy. Meteor. Soc.*, **143**, 2862–2873, https://doi.org/10.1002/qj.3136.

Skamarock, W. C., 2004: Evaluating mesoscale NWP models using kinetic energy spectra. *Mon. Wea. Rev.*, **132**, 3019–3032, https://doi.org/10.1175/MWR2830.1.

——, and Coauthors, 2019: A description of the Advanced Research WRF Model version 4. NCAR Tech. Note NCAR/TN-556+STR, 145 pp., https://doi.org/10.5065/1dfh-6p97.

Smirnova, T. G., J. M. Brown, and D. Kim, 2000: Parameterization of cold-season processes in the MAPS land-surface scheme. *J. Geophys. Res.*, **105**, 4077–4086, https://doi.org/10.1029/1999JD901047.

——, ——, S. G. Benjamin, and J. S. Kenyon, 2016: Modifications to the Rapid Update Cycle Land Surface Model (RUC LSM) available in the Weather Research and Forecasting Model. *Mon. Wea. Rev.*, **144**, 1851–1865, https://doi.org/10.1175/MWR-D-15-0198.1.

Smith, T. L., S. G. Benjamin, J. M. Brown, S. Weygandt, T. Smirnova, and B. Schwartz, 2008: Convection forecasts from the hourly updated, 3-km High-Resolution Rapid Refresh (HRRR) model. *24th Conf. on Severe Local Storms,* Savannah, GA, Amer. Meteor. Soc., 11.1, https://ams.confex.com/ams/pdfpapers/142055.pdf.

Smith, T. M., and Coauthors, 2016: Multi-Radar Multi-Sensor (MRMS) severe weather and aviation products: Initial operating capabilities. *Bull. Amer. Meteor. Soc.*, **97**, 1617–1630, https://doi.org/10.1175/BAMS-D-14-00173.1.

Stensrud, D. J., and Coauthors, 2009: Convective-scale Warn-on-Forecast System: A vision for 2020. *Bull. Amer. Meteor. Soc.*, **90**, 1487–1499, https://doi.org/10.1175/2009BAMS2795.1.

Sun, J., and Coauthors, 2014: Use of NWP for nowcasting convective precipitation: Recent progress and challenges. *Bull. Amer. Meteor. Soc.*, **95**, 409–426, https://doi.org/10.1175/BAMS-D-11-00263.1.

Tang, Y., H. W. Lean, and J. Bornemann, 2013: The benefits of the Met Office variable resolution NWP model for forecasting convection. *Meteor. Appl.*, **20**, 417–426, https://doi.org/10.1002/met.1300.

Thompson, G., and T. Eidhammer, 2014: A study of aerosol impacts on clouds and precipitation development in a large winter cyclone. *J. Atmos. Sci.*, **71**, 3636–3658, https://doi.org/10.1175/JAS-D-13-0305.1.

——, R. M. Rasmussen, and K. Manning, 2004: Explicit forecasts of winter precipitation using an improved bulk microphysics scheme. Part I: Description and sensitivity

analysis. *Mon. Wea. Rev.*, **132**, 519–542, https://doi.org/10.1175/1520-0493(2004)132<0519:EFOWPU>2.0.CO;2.

——, P. R. Field, R. M. Rasmussen, and W. D. Hall, 2008: Explicit forecasts of winter precipitation using an improved bulk microphysics scheme. Part II: Implementation of a new snow parameterization. *Mon. Wea. Rev.*, **136**, 5095–5115, https://doi.org/10.1175/2008MWR2387.1.

Tippett, M. K., J. L. Anderson, C. H. Bishop, T. M. Hamill, and J. S. Whitaker, 2003: Ensemble square root filters. *Mon. Wea. Rev.*, **131**, 1485–1490, https://doi.org/10.1175/1520-0493(2003)131<1485:ESRF>2.0.CO;2.

Torn, R. D., G. J. Hakim, and C. Snyder, 2006: Boundary conditions for limited-area ensemble Kalman filters. *Mon. Wea. Rev.*, **134**, 2490–2502, https://doi.org/10.1175/MWR3187.1.

Trahan, S., and L. Sparling, 2012: An analysis of NCEP tropical cyclone vitals and potential effects on forecasting models. *Wea. Forecasting*, **27**, 744–756, https://doi.org/10.1175/WAF-D-11-00063.1.

Tsiringakis, A., G. J. Steenveld, and A. A. M. Holtslag, 2017: Small-scale orographic gravity wave drag in stable boundary layers and its impact on synoptic systems and near-surface meteorology. *Quart. J. Roy. Meteor. Soc.*, **143**, 1504–1516, https://doi.org/10.1002/qj.3021.

Turner, D. D., and Coauthors, 2007: Thin liquid water clouds: Their importance and our challenge. *Bull. Amer. Meteor. Soc.*, **88**, 177–190, https://doi.org/10.1175/BAMS-88-2-177.

——, H. Cutler, M. Shields, R. Hill, B. Hartman, Y. Hu, T. Lu, and H. Jeon, 2022: Evaluating the economic impacts of improvements to the High-Resolution Rapid Refresh (HRRR) numerical weather prediction model. *Bull. Amer. Meteor. Soc.*, **103**, E198–E211, https://doi.org/10.1175/BAMS-D-20-0099.1.

Uccellini, L. W., 2013: Introduction to Sandy and the major impacts. *Town Hall Meeting: Hurricane and Post-Tropical Cyclone Sandy: Predictions, Warnings, Societal Impacts and Responses,* Austin, TX, Amer. Meteor. Soc., https://ams.confex.com/ams/93Annual/recordingredirect.cgi/id/23244.

Wang, W., X. Liu, J. Bi, and Y. Liu, 2022: A machine learning model to estimate ground-level ozone concentrations in California using TROPOMI data and high-resolution meteorology. *Environ. Int.*, **158**, 106917, https://doi.org/10.1016/j.envint.2021.106917.

Wang, X., and T. Lei, 2014: GSI-based four-dimensional ensemble-variational (4DEnsVar) data assimilation: Formulation and single-resolution experiments with real data for NCEP Global Forecast System. *Mon. Wea. Rev.*, **142**, 3303–3325, https://doi.org/10.1175/MWR-D-13-00303.1.

——, D. Parrish, D. Kleist, and J. Whitaker, 2013: GSI 3DVar-based ensemble-variational hybrid data assimilation for NCEP Global Forecast System: Single-resolution experiments. *Mon. Wea. Rev.*, **141**, 4098–4117, https://doi.org/10.1175/MWR-D-12-00141.1.

Wang, Y., and X. Wang, 2021: Development of convective-scale static background error covariance within GSI-based hybrid EnVar system for direct radar reflectivity data assimilation. *Mon. Wea. Rev.*, **149**, 2713–2736, https://doi.org/10.1175/MWR-D-20-0215.1.

——, J. Huang, T. J. Zananski, P. K. Hopke, and T. M. Holsen, 2010: Impacts of the Canadian forest fires on atmospheric mercury and carbonaceous particles in Northern New York. *Environ. Sci. Technol.*, **44**, 8435–8440, https://doi.org/10.1021/es1024806.

Wattrelot, E., O. Caumont, and J.-F. Mahfouf, 2014: Operational implementation of the 1D+3D- Var assimilation of radar reflectivity data in the AROME model. *Mon. Wea. Rev.*, **142**, 1852–1873, https://doi.org/10.1175/MWR-D-13-00230.1.

Weisman, M. L., W. C. Skamarock, and J. B. Klemp, 1997: The resolution dependence of explicitly modeled convective systems. *Mon. Wea. Rev.*, **125**, 527–548, https://doi.org/10.1175/1520-0493(1997)125<0527:TRDOEM>2.0.CO;2.

——, C. Davis, W. Wang, K. W. Manning, and J. B. Klemp, 2008: Experiences with 0–36-h explicit convective forecasts with the WRF-ARW model. *Wea. Forecasting*, **23**, 407–437, https://doi.org/10.1175/2007WAF2007005.1.

Weygandt, S. S., S. G. Benjamin, M. Hu, C. R. Alexander, T. G. Smirnova, and E. P. James, 2022: Radar reflectivity-based model initialization using specified latent heating (Radar-LHI) within a diabatic digital filter or pre-forecast integration. *Wea. Forecasting*, in press, https://doi.org/10.1175/WAF-D-21-0142.1.

Whitaker, J. S., and T. M. Hamill, 2012: Evaluating methods to account for system errors in ensemble data assimilation. *Mon. Wea. Rev.*, **140**, 3078–3089, https://doi.org/10.1175/MWR-D-11-00276.1.

——, ——, X. Wei, Y. Song, and Z. Toth, 2008: Ensemble data assimilation with the NCEP Global Forecast System. *Mon. Wea. Rev.*, **136**, 463–482, https://doi.org/10.1175/2007MWR2018.1.

Wicker, L. J., and W. C. Skamarock, 2020: An implicit-explicit vertical transport scheme for convection allowing models. *Mon. Wea. Rev.*, **149**, 3893–3910, https://doi.org/10.1175/MWR-D-20-0055.1.

Wolfson, M. M., W. J. Dupree, R. M. Rasmussen, M. Steiner, S. G. Benjamin, and S. S. Weygandt, 2008: Consolidated Storm Prediction for Aviation (CoSPA). *13th Conf. on Aviation, Range, and Aerospace Meteorology*, New Orleans, LA, Amer. Meteor. Soc., J6.5, https://ams.confex.com/ams/88Annual/webprogram/Paper132981.html.

Wu, W.-S., R. J. Purser, and D. F. Parrish, 2002: Three-dimensional variational analysis with spatially inhomogeneous covariances. *Mon. Wea. Rev.*, **130**, 2905–2916, https://doi.org/10.1175/1520-0493(2002)130<2905:TDVAWS>2.0.CO;2.

Wu, Y., A. Arapi, J. Huang, B. Gross, and F. Moshary, 2018: Intra-continental wildfire smoke transport and impact on local air quality observed by ground-based and satellite remote sensing in New York City. *Atmos. Environ.*, **187**, 266–281, https://doi.org/10.1016/j.atmosenv.2018.06.006.

Xu, K.-M., and D. A. Randall, 1996: A semiempirical cloudiness parameterization for use in climate models. *J. Atmos. Sci.*, **53**, 3084–3102, https://doi.org/10.1175/1520-0469(1996)053<3084:ASCPFU>2.0.CO;2.

Xue, M., 2000: High-order monotonic numerical diffusion and smoothing. *Mon. Wea. Rev.*, **128**, 2853–2864, https://doi.org/10.1175/1520-0493(2000)128<2853:HOMNDA>2.0.CO;2.

Zeng, X., M. Shaikh, Y. Dai, R. E. Dickinson, and R. Myneni, 2002: Coupling of the common land model to the NCAR Community Climate Model. *J. Climate*, **15**, 1832–1854, https://doi.org/10.1175/1520-0442(2002)015<1832:COTCLM>2.0.CO;2.

Zhang, J., and Coauthors, 2016: Multi-Radar Multi-Sensor (MRMS) quantitative precipitation estimation: Initial operating capabilities. *Bull. Amer. Meteor. Soc.*, **97**, 621–637, https://doi.org/10.1175/BAMS-D-14-00174.1.